WIND PRESSURES AND FORCES ON FLAT-PLATE PHOTOVOLTAIC SOLAR ARRAYS--CROSS-SPECTRAL ANALYSIS

by

N. Hosoya,* J. A. Peterka,**
and J. E. Cermak***

for

Boeing Engineering and Construction Company
P.O. Box 3707
Seattle, Washington 98124

Fluid Dynamics and Diffusion Laboratory
Civil Engineering Department
Colorado State University
Fort Collins, Colorado 80523
Project 5-36022

June 1981

*Graduate Research Assistant
**Associate Professor
***Professor-in-Charge, Fluid Mechanics
and Wind Engineering Program

CER80-81NH-JAP-JEC57

TABLE OF CONTENTS

LIST OF FIGURES

LIST OF TABLES

LIST OF SYMBOLS

Symbol	Definition
c	chord length of solar array (4 in model, 8 ft full-scale)
C_M	pitching moment coefficient
C_N	normal force coefficient
C_p	instantaneous pressure coefficient
C_p'	fluctuation of pressure coefficient
$C_{p_{mean}}$	mean pressure coefficient
$C_{p_{rms}}$	root-mean-square of pressure coefficient
e	eccentricity of center of pressure from mid-chord
FN	normal force per unit area
H_f	fence height
M	pitching moment per unit area about center of chord
N	frequency
N*	normalized frequency $= \frac{N \cdot c}{U_{ref}}$
P	local pressure on collector
ΔP	pressure difference across collector
q_{ref}	reference dynamic pressure at 10 m full-scale
$R_{ij}(\tau)$	correlation function
U_{ref}	reference wind velocity (approx. 43 fps model) at 10 m height
x_f	fence distance
α	angle of attack
τ	time lag
$\Phi_{ij}(N)$	power spectral function
$\Phi_{ij}^*(N^*)$	normalized power spectral function

PREFACE

Simultaneous pressure measurements on flat plate photovoltaic solar arrays were conducted in a simulated atmospheric boundary layer characterized by a 1/7th power law mean velocity distribution. This report describes random properties of fluctuating local pressures on solar arrays by cross-spectral analysis. The random properties to be analyzed include the auto- and cross-spectra for fluctuating pressures for several typical array configurations.

The essential experimental configurations, including facilities, wind-tunnel models, instrumentation and the flow simulation technique, have been described in a preceding report [5] "Wind Pressures and Forces on Flat-Plate Photovoltaic Solar Arrays," Colorado State University Report CER80-81NH-JAP-MP-JEC13. The simultaneous pressure measurements presented in this supplementary report required some additional arrangements for instrumentation and data acquisition. These arrangements will be described in Sections 1 and 2 of this report.

1.0 PRESSURE TAPS AND ARRAY CONFIGURATIONS

1.1 Pressure Taps

The simultaneous pressure measurements were obtained at four pressure taps along the chord on the upstream surface and four pressure taps on the downstream surface of the solar array. These pressure taps tested were taps 1, 4, 7 and 10 on the upstream surface, and taps 11, 14, 17 and 20 on the downstream surface. The location of each pressure tap is shown in Figure 1 which duplicates Figure 10 of the preceding report.

1.2 Array Configurations

All array configurations tested for this phase of the study are listed in Table 1. Array locations are shown in Figure 2 which duplicates Figure 11 in the preceding report. Several typical array configurations are chosen to be presented and discussed in this report. For this study, the ground clearance and spacing of solar arrays were 0.25 c and 2.0 c respectively, and were not varied. The wind direction was 0° for all array configurations. The definitions of these test parameters are seen in Figure 2.

2.0 DATA ACQUISITION

The mean wind velocity outside the simulated turbulent boundary layer in the Meteorological Wind Tunnel, shown in Figure 1 of the main report, was approximately 50 fps as was used for the preceding tests (giving a $U_{ref} \simeq 43$ fps). The outputs from the 8 pressure transducers were recorded simultaneously on digital magnetic tape for 35 seconds at 500 samples per second using a data acquisition system based on a Hewlett-Packard System 1000 minicomputer. The data were then analyzed by the same computer. Pressure, normal force and pitching moment coefficients presented in this report were referenced to the mean dynamic pressure at 10 m elevation in the prototype. The power spectral densities of local peak pressures were evaluated with these pressure coefficients.

2.1 Pressure and Normal Force Coefficients

Pressure and normal force coefficients are respectively defined in Sections 3.2 and 3.3 of the preceding report. The same definitions apply to this report:

$$C_p = \frac{P}{q_{ref}} \quad , \quad \Delta C_p = \frac{\Delta P}{q_{ref}}$$
$$C_N = \frac{1}{c}\int_0^c \Delta C_p(s)\,ds \tag{1}$$

2.2 Pitching Moment Coefficients

Pitching moment coefficients, C_M, about the mid-chord of the solar array are defined by

$$C_M = \frac{M}{q_{ref} \cdot c} \tag{2}$$

where M is the calculated pitching moment per unit surface area about the mid-chord of the array, q_{ref} is the reference dynamic pressure of approaching flow at 10 m full-scale, and c is the chord length of the array. In order to calculate M, the eccentricity of the center of pressure, e, was obtained numerically by a curve fitting to the pressure distribution using linear interpolation schemes along the chord of the array. Thus

$$M^* = FN \cdot e \tag{3}$$

where FN is the normal force.

*pitching moment lifting windward edge up is defined to be positive.

2.3 Spectral Analysis

2.3.1 Matrix Arrangement

A set of cross-power spectral densities of local pressure fluctuations on the solar array were calculated. For simplicity of notation, the pressure tap numbers 1,4,7,10,11,14,17 and 20 can be renamed as 1,2,3,...,8 in order. Any pressure tap number used in this report will be, hereafter, referred to as the renamed one.

Matrices for the correlation and power spectral densities are written as follows.

$$\left[R_{ij}(\tau) \right] = \begin{cases} \text{auto-correlation}, & \text{if } i = j \\ \text{cross-correlation}, & \text{if } i \neq j \end{cases}$$

$$\left[\Phi_{ij}(N) \right] = \begin{cases} \text{auto-spectrum}, & \text{if } i = j \\ \text{cross-spectrum}, & \text{if } i \neq j \end{cases}$$

where τ is time lag, N is frequency, and i,j refer to the pressure tap numbers.

2.3.2 Correlation Functions

For this analysis, auto- and cross-correlation functions are defined by

$$R_{ij}(\tau) = \lim_{T\to\infty} \frac{1}{T} \int_0^T \left[C_{p_i}(t) - C_{p_{mean_i}} \right] \left[C_{p_j}(t+\tau) - C_{p_{mean_j}} \right] d\tau \tag{4}$$

where $C_{p_k}(t)$ and $C_{p_{mean_k}}$ are instantaneous and time-averaged values of pressure coefficient with respect to tap number k. Defining a fluctuating component of pressure coefficient, $C'_{p_k}(t)$, as

$$C'_{p_k}(t) = C_{p_k}(t) - C_{p_{mean_k}} \tag{5}$$

the auto-correlation function, at $\tau = 0$, becomes for one tap

$$R_{ii}(0) = \overline{C'_{p_i}(t)\, C'_{p_i}(t)} = C^2_{p_{rms_i}} \tag{6}$$

in which an overbar denotes a time averaging.

2.3.3 Power Spectral Density Functions

Power spectral density functions are defined by

$$\Phi_{ij}(N) = 4 \int_0^\infty R_{ij}(\tau)\, \exp(-j2\pi N\tau)\, d\tau \tag{7}$$

where j appearing in the exponential function refers to $j^2 = -1$.

The integral property of the auto-spectral function requires

$$\int_0^\infty \Phi_{ii}(N)\, dN = R_{ii}(0) = C^2_{p_{rms_i}} \tag{8}$$

Because of this property, the power spectral density can be normalized by

$$\Phi^*_{ij}(N) = \frac{|\Phi_{ij}(N)|}{C_{p_{rms_i}} \cdot C_{p_{rms_j}}} \quad \text{with units } \left[\frac{1}{\text{Hz}}\right] \tag{9}$$

It is also common practice to normalize the frequency N by

$$N^* = \frac{Nc}{U_{ref}} \tag{10}$$

where U_{ref} is the reference wind velocity.

The cross-spectral analysis was performed digitally by a Fourier Transform subroutine using standard techniques such as those in references [1] and [3]. Transforms were performed on 8 time segments, each 2048 samples in length, for each pressure record (recorded at

500 samples per second). Transforms were combined to form cross-spectra and appropriate averaging across data points in frequency and time segments was performed to reduce normalized standard error of the spectrum. Because of memory limitations, the cross-spectra were only calculated to a maximum frequency of 125 Hz ($N^* \simeq 1.0$). This frequency retained virtually all the energy in the fluctuating pressures. Normalized standard error of the cross-spectra reached a maximum of 11 percent at the lower frequencies.

3.0 RESULTS AND DISCUSSIONS

3.1 Pressure and Normal Force Coefficients

Examples of time traces of normal force and pitching moment coefficients are shown in Figure 3 obtained with the first solar array at $\alpha = 35°$, without fence. The time-averaged mean and rms pressure coefficients are tabulated in Table 2 for six typical array configurations, including Runs 21331, 21344, 21346, 21352 and 21368. These values agree well with those found in the preceding report [5].

3.2 Power Spectral Analysis

The auto-spectra for each pressure tap are shown in Figures 4 through 9 for the six cases listed in Table 2. Comparing the auto-spectra for the individual pressure taps and for both surfaces of the solar array, the power spectra show that the energy is shifted to higher frequencies for the first array with fence and the fifth array, consistent with the smaller scales of turbulence expected behind the fence and within the array field. The rear side of the first array also shows this effect. The area under the auto-spectra over the available frequency range is compared to the measured variance in fluctuating pressure in Table 3. Figures 4 through 9 clearly show that the energy content in the power spectra is concentrated at $N^* < 0.1$. At $N^* \simeq 0.3$, a spike in the power spectra is seen for both the upstream and downstream surfaces. This spike in the power spectra is due to vibration of the wind-tunnel model. Moreover, for some cases, another spike at $N^* \simeq 0.4$ was obtained which is a second mode of vibration of the model. No attempt was made to model the full-scale structural stiffness or damping so that these response spikes do not indicate full-scale response.

Both the real and imaginary parts of the auto- and the cross-spectra were calculated. Only the real part is shown in Figures 4 through 9. The imaginary part was essentially zero for all cases. The implication of this finding is that the phase angles of the various frequencies are uncorrelated. This is a typical result in velocity or pressure fluctuations in turbulent boundary layer flows.

Figures 10 through 15 show cross-spectral plots for all combinations of taps for each of the six cases listed in Table 2. Cross-spectra for each array were grouped on plots so that similarly-shaped curves would appear on the same plot. The plots reveal the same increase in energy at higher frequencies for arrays behind the fence and within the array field as was observed for the auto-spectra. Also, the model natural frequency of vibration shows in the plots.

4.0 CONCLUSIONS

On the basis of the data presented in previous sections, the following conclusions can be drawn.

1. Auto-spectra of local pressure fluctuations characteristically fall rapidly with increasing frequency.

2. Auto-spectra show higher energy at the higher frequencies where the pressure tap is within the array field or behind a wind fence.

3. Cross-spectra showed properties similar to those in 1 and 2 above.

4. Cross-spectra between taps in separated zones were quite similar.

5. The imaginary parts of both auto- and cross-spectra were essentially zero.

REFERENCES

1. Akins, R. E. and J. A. Peterka, "Computation of Power Spectral Densities and Correlations Using Digital FFT Techniques," (1975), Colorado State University Report CER75-76REA-JAP13, Fort Collins.

2. Bearman, P. W., "Wind Loads on Structures in Turbulent Flow," (1971), Proc. Modern Design of Wind Sensitive Structures, Paper 4, pp. 57-64.

3. Bendat, J. S. and A. G. Piersol, "Random Data: Analysis and Measurement Procedures," (1971), John Wiley and Sons Inc.

4. Cermak, J. E., "Aerodynamics of Buildings," (1976), Annual Review of Fluid Mechanics, Vol. 8, pp. 75-106.

5. Hosoya, N., J. A. Peterka, M. Poreh, and J. E. Cermak, "Wind Forces and Pressures on Flat-Plate Photovoltaic Solar Arrays," (1980), Fluid Mechanics and Wind Engineering Program, Colorado State University Report CER80-81NH-JAP-MP-JEC13, Fort Collins, September.

FIGURES

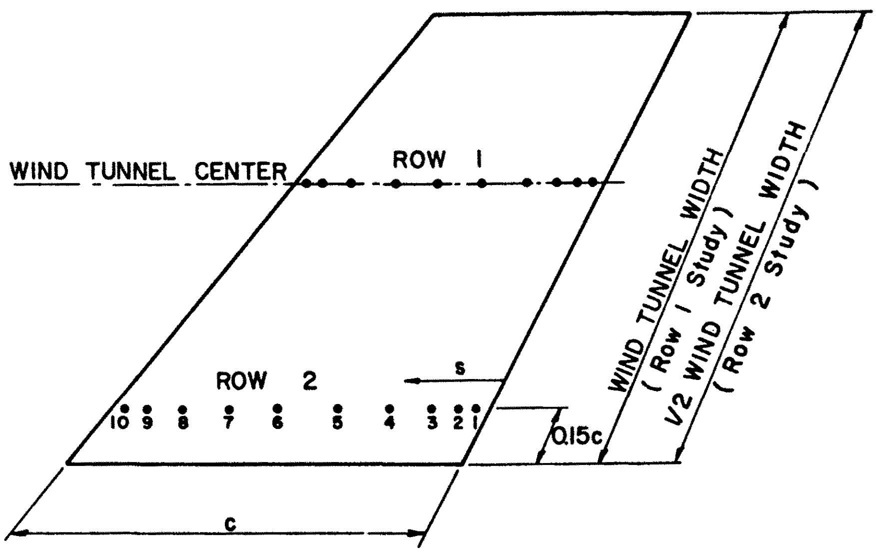

TAP LOCATIONS - FRACTION OF CHORD s/c

	1	2	3	4	5	6	7	8	9	10
UPSTREAM SURFACE	0.052	0.102	0.172	0.272	0.432	0.592	0.752	0.852	0.922	0.972
DOWNSTREAM SURFACE	0.028	0.078	0.148	0.248	0.408	0.568	0.728	0.828	0.898	0.948

Figure 1. Position of Pressure Taps on Instrumented Model

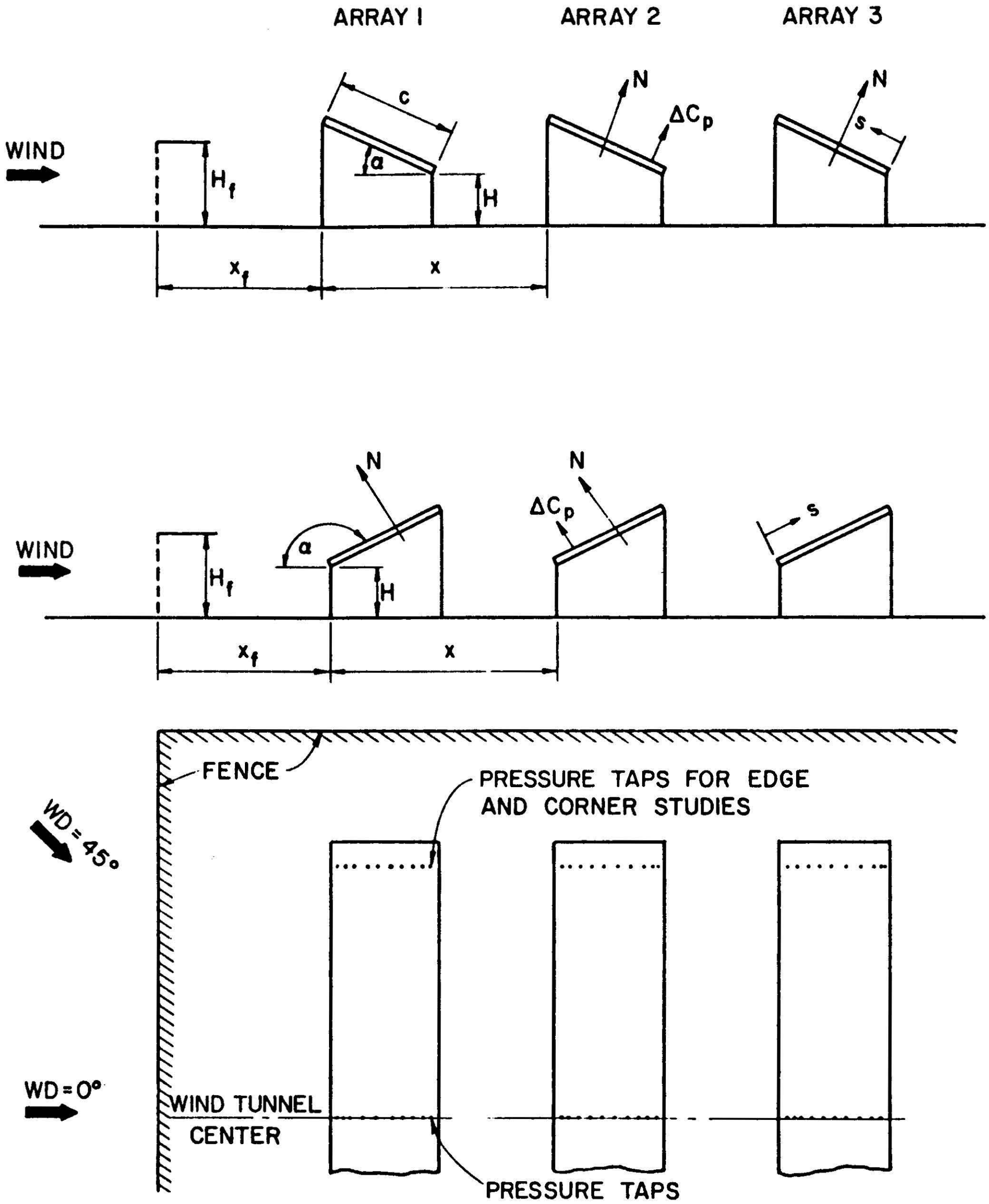

Figure 2. Schematic Description of Array Field

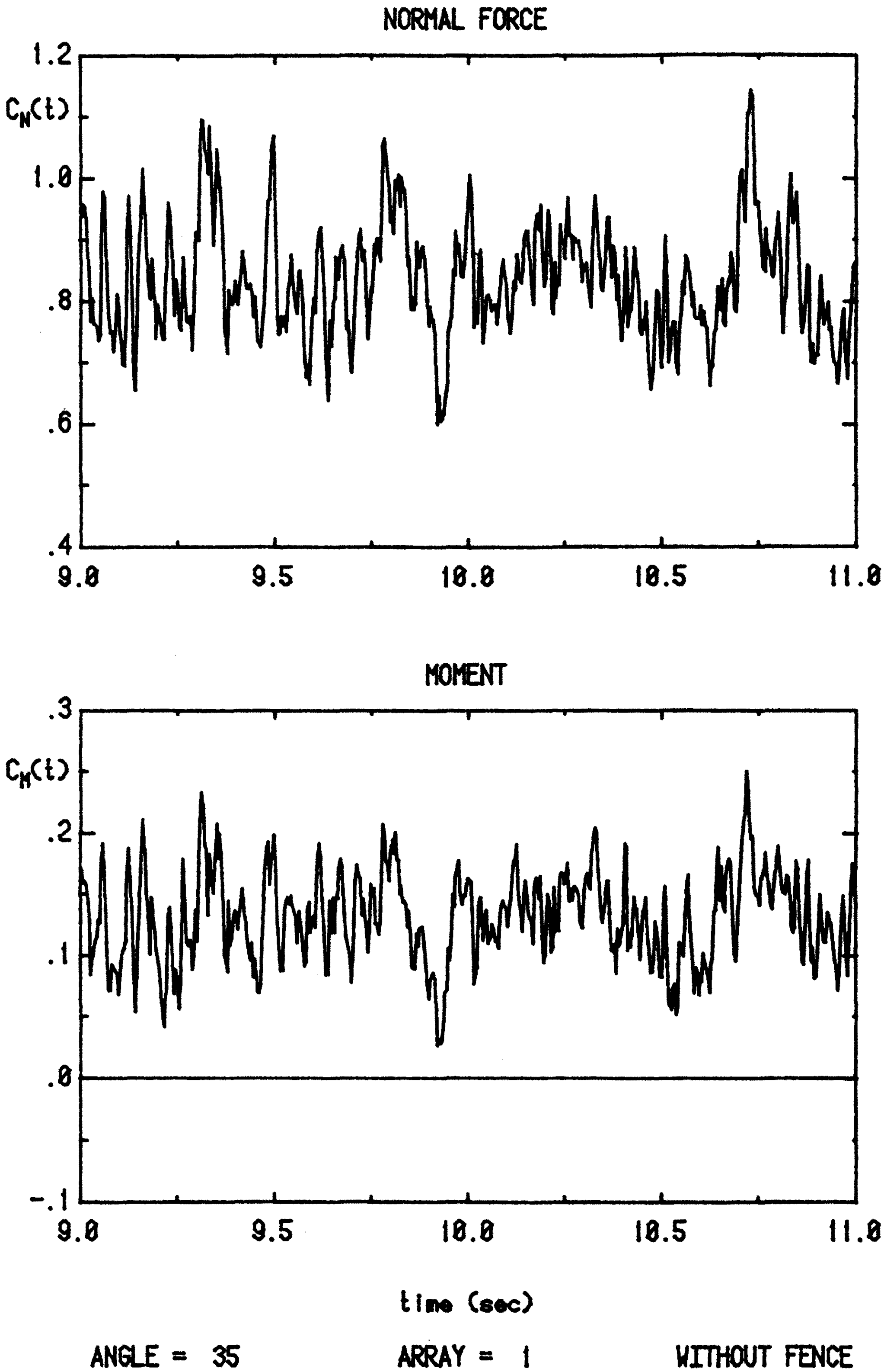

Figure 3. Time Trace of the Normal Force and Pitching Moment Coefficients

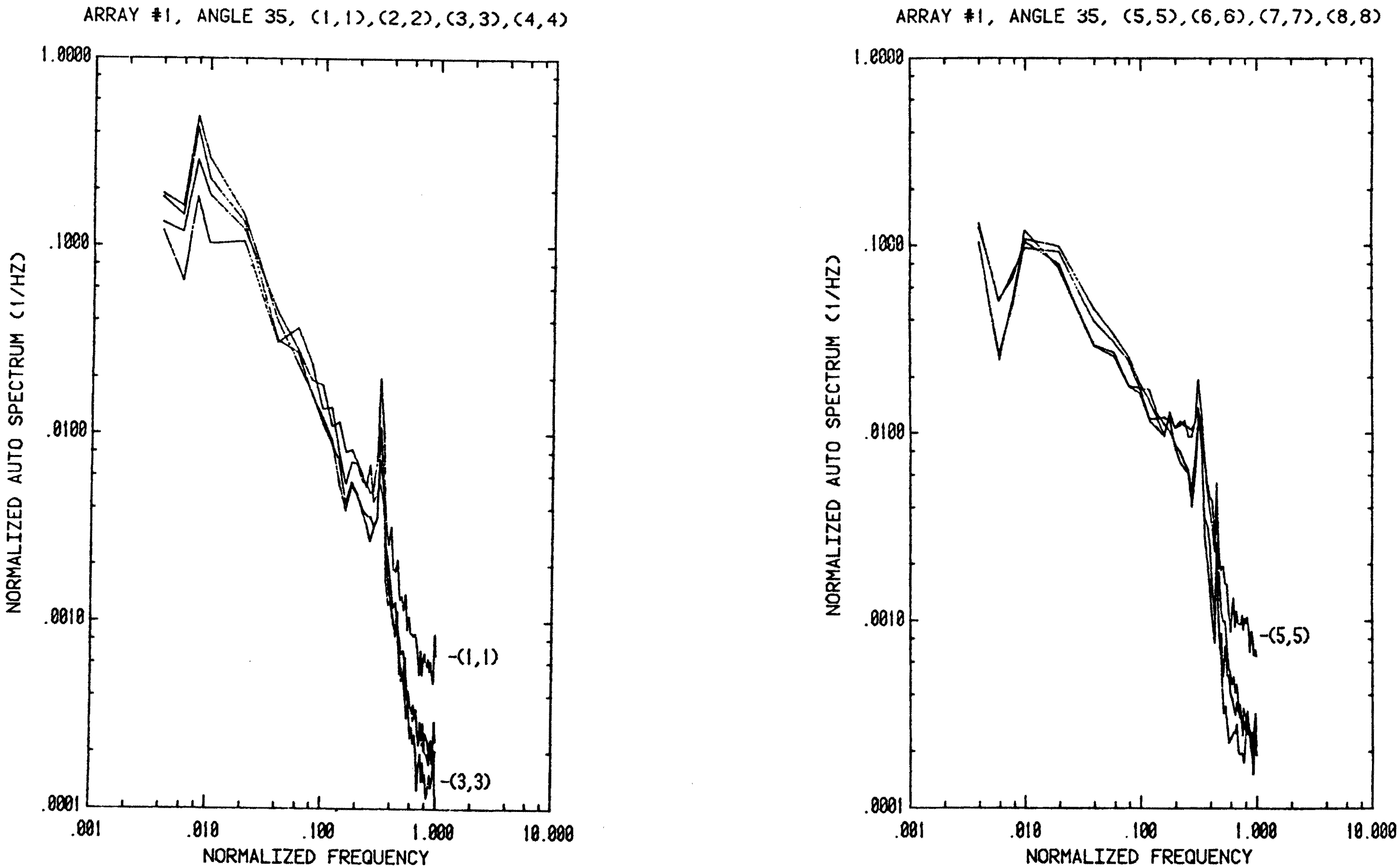

Figure 4. Auto-Spectra for First Array at α = 35°, without Fence

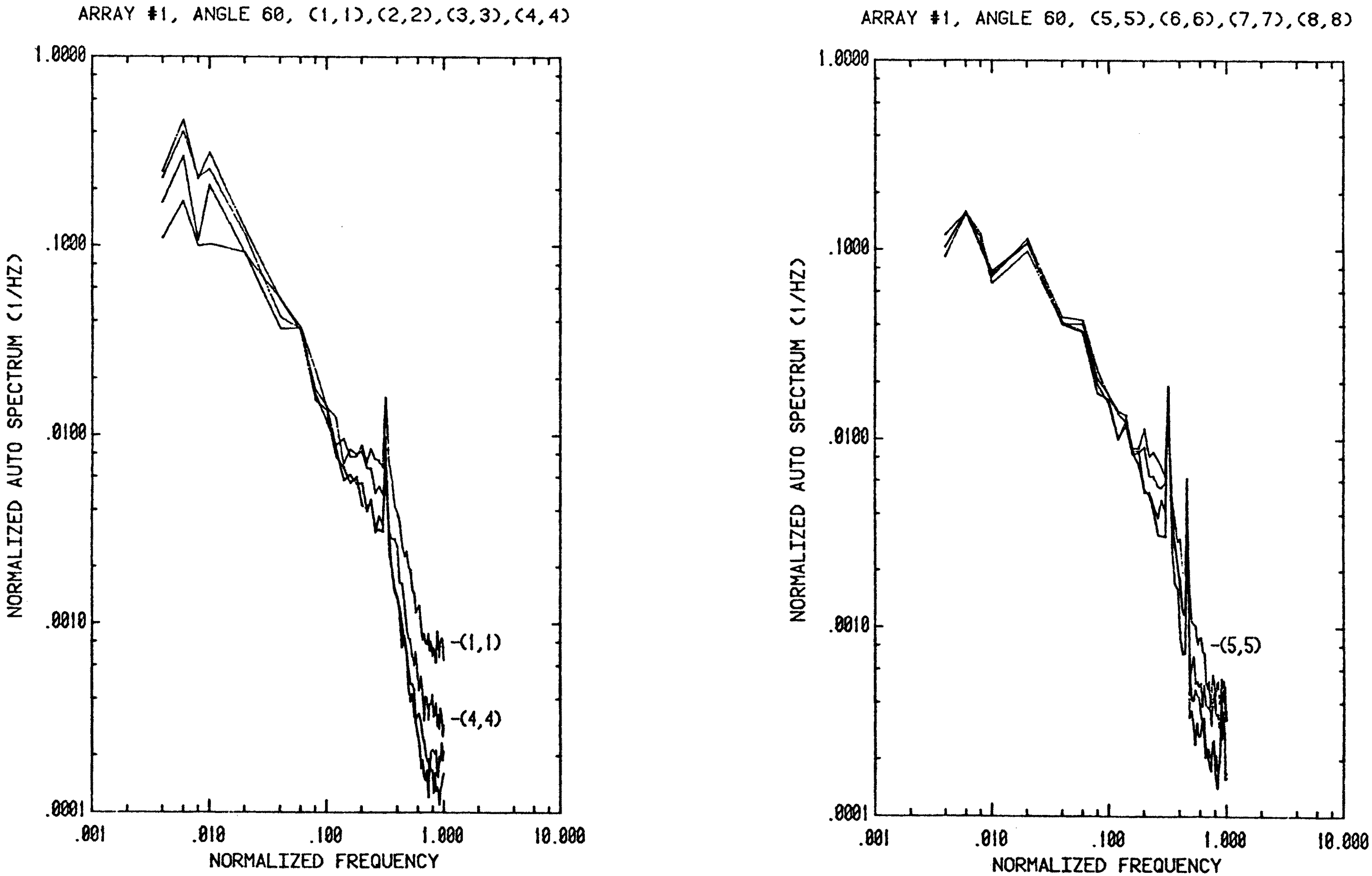

Figure 5. Auto-Spectra for First Array at $\alpha = 60°$, without Fence

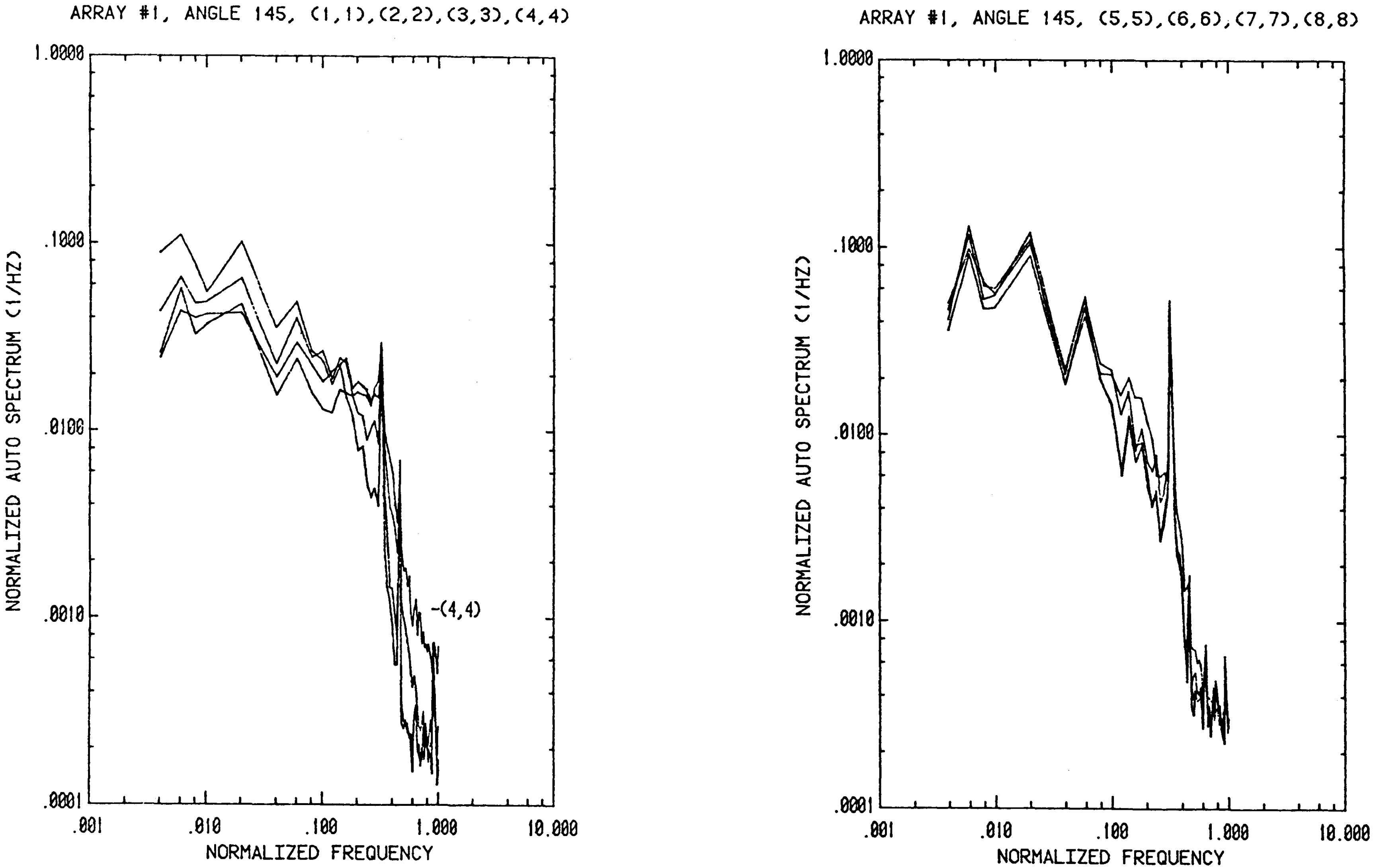

Figure 6. Auto-Spectra for First Array at $\alpha = 145°$, with Fence

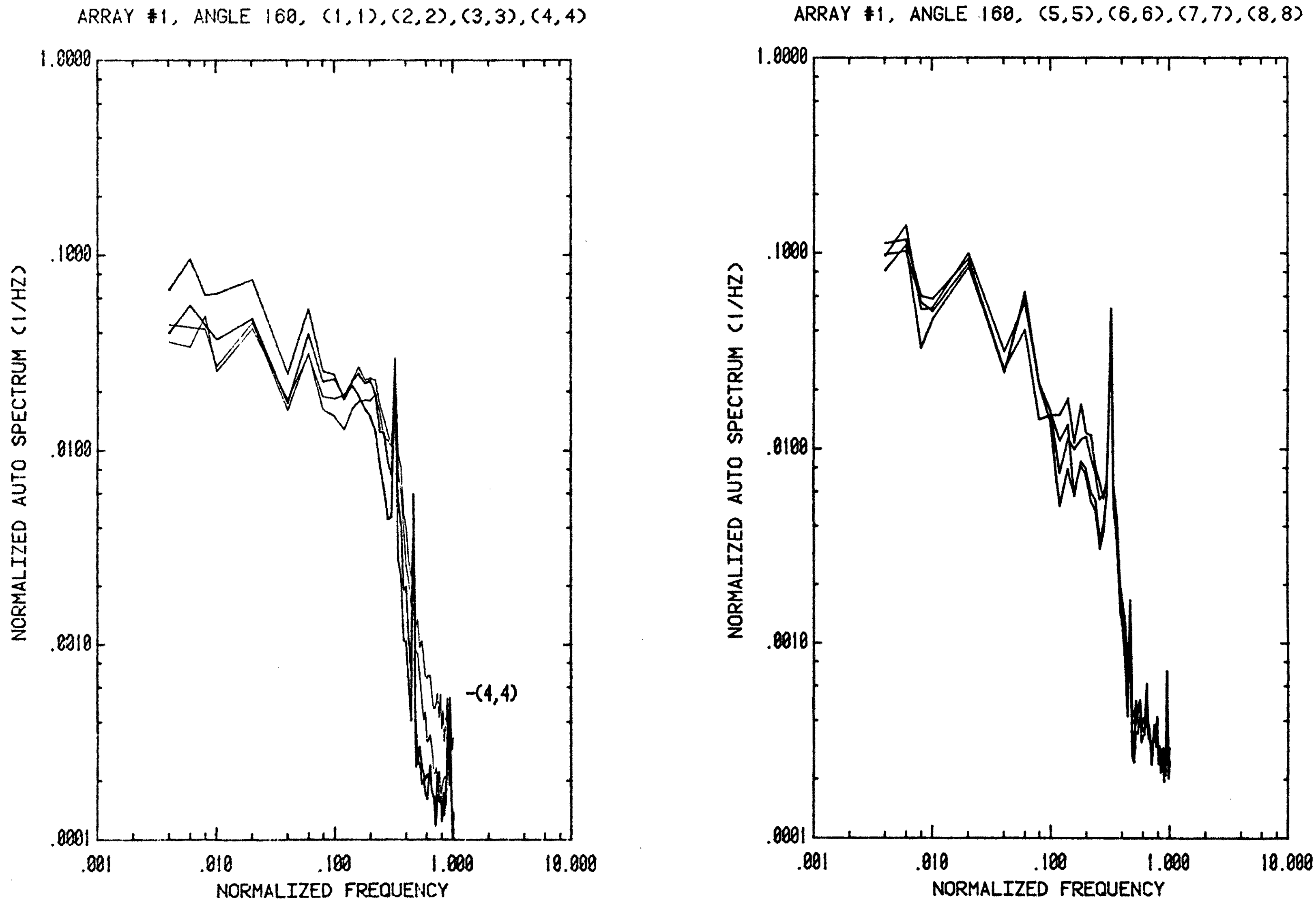

Figure 7. Auto-Spectra for First Array at $\alpha = 160°$, with Fence

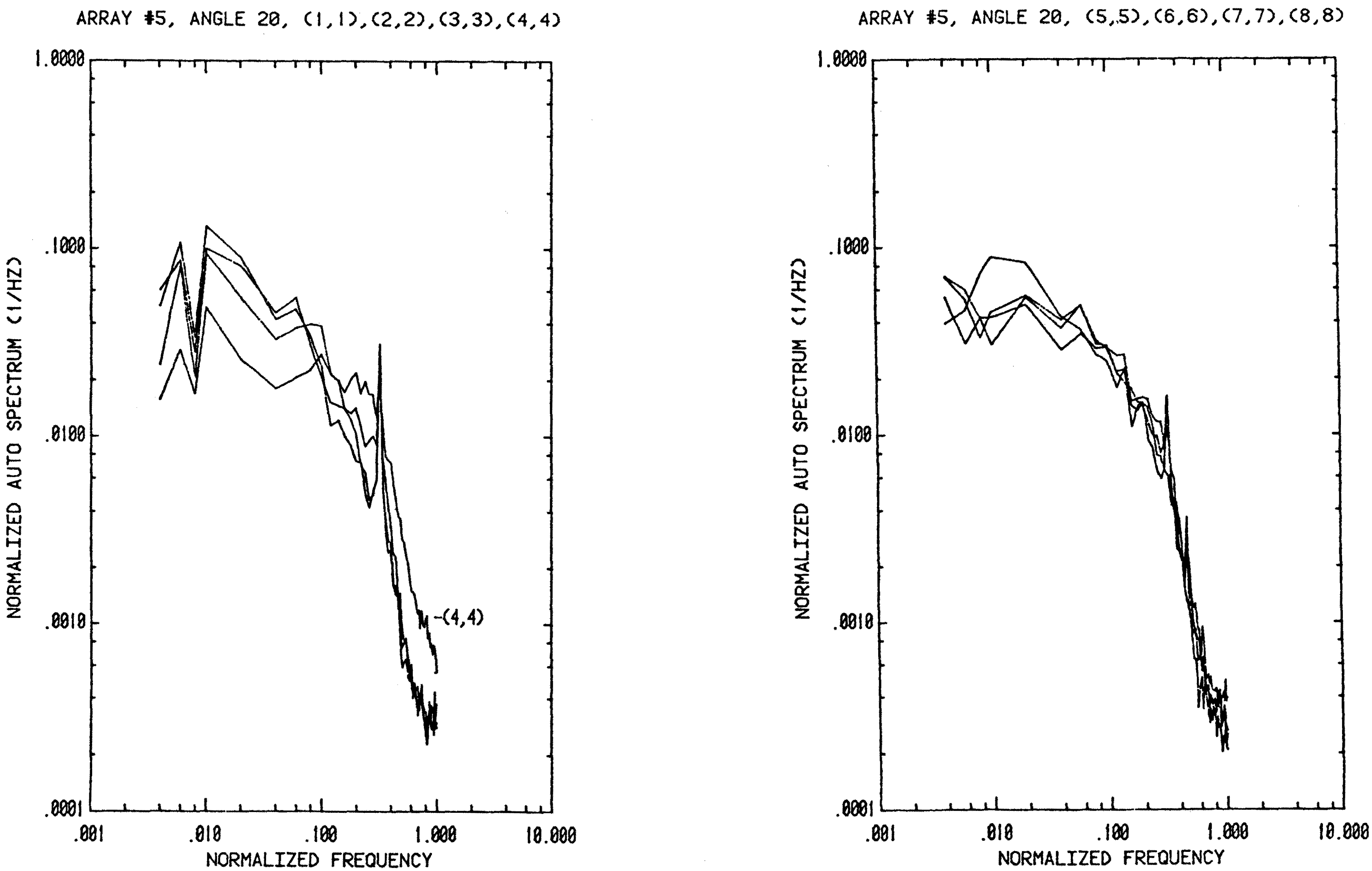

Figure 8. Auto-Spectra for Fifth Array at $\alpha = 20°$, without Fence

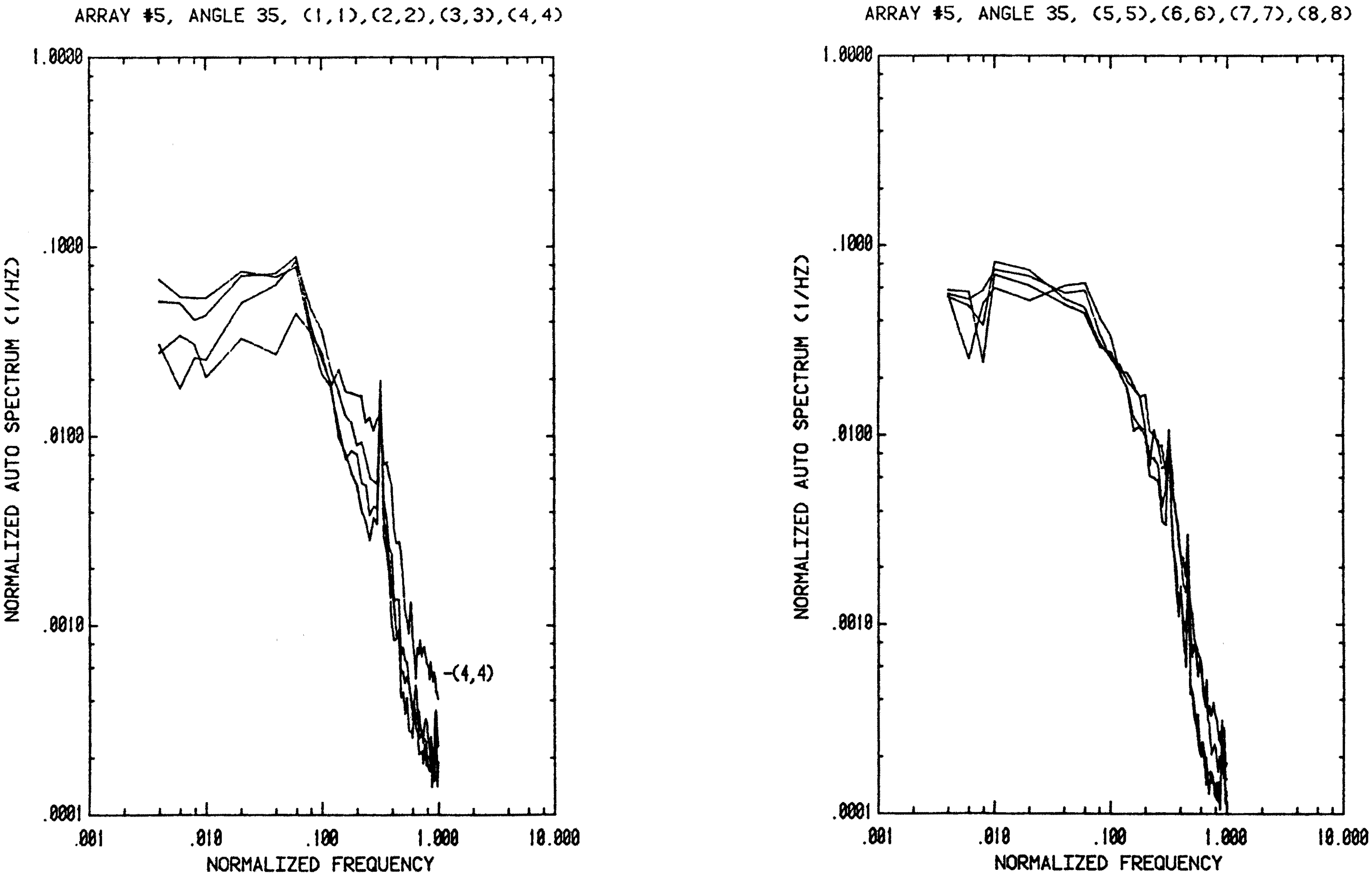

Figure 9. Auto-Spectra for Fifth Array at α = 35°, without Fence

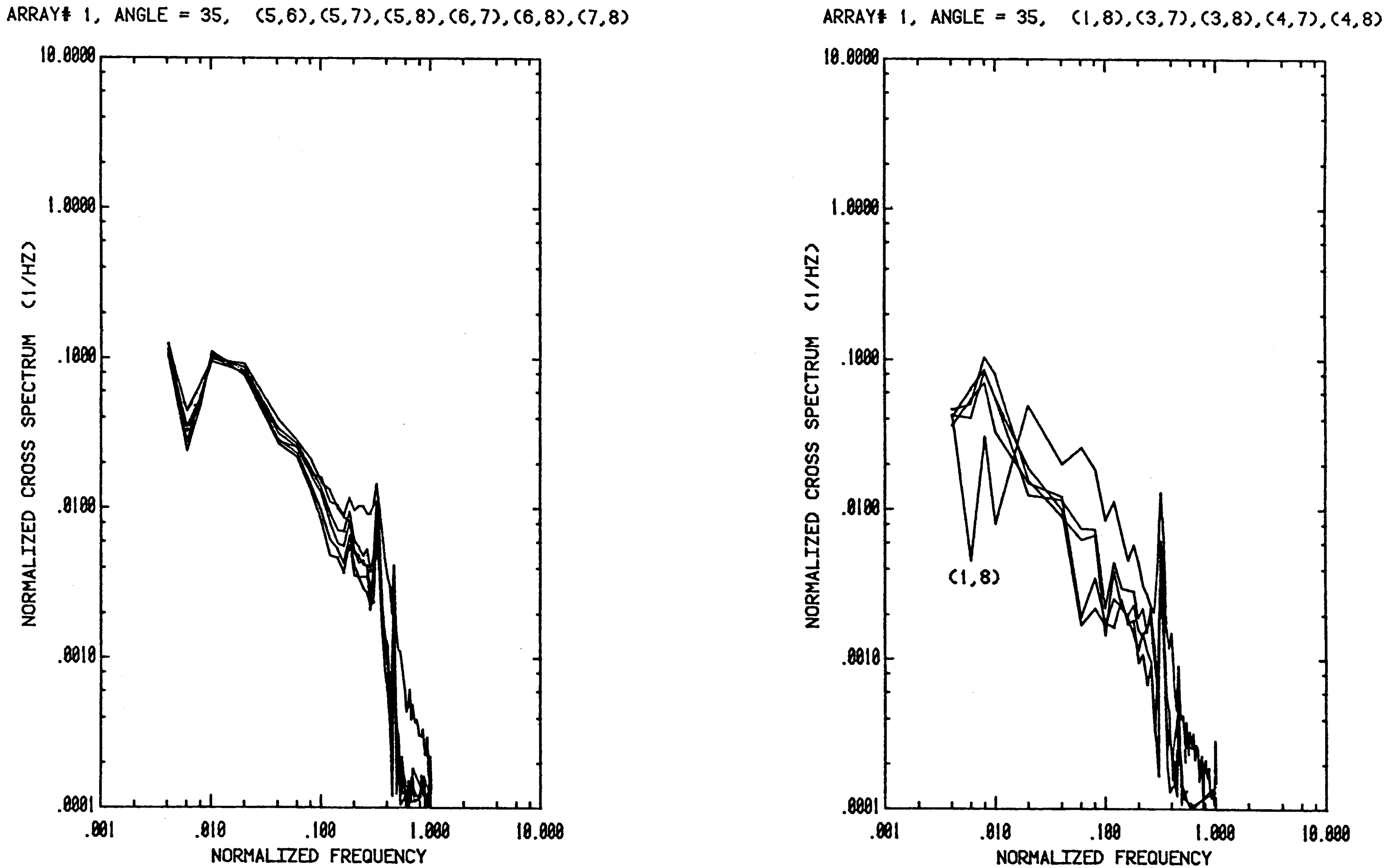

Figure 10. Cross-Spectra for First Array at $\alpha = 35°$, without Fence

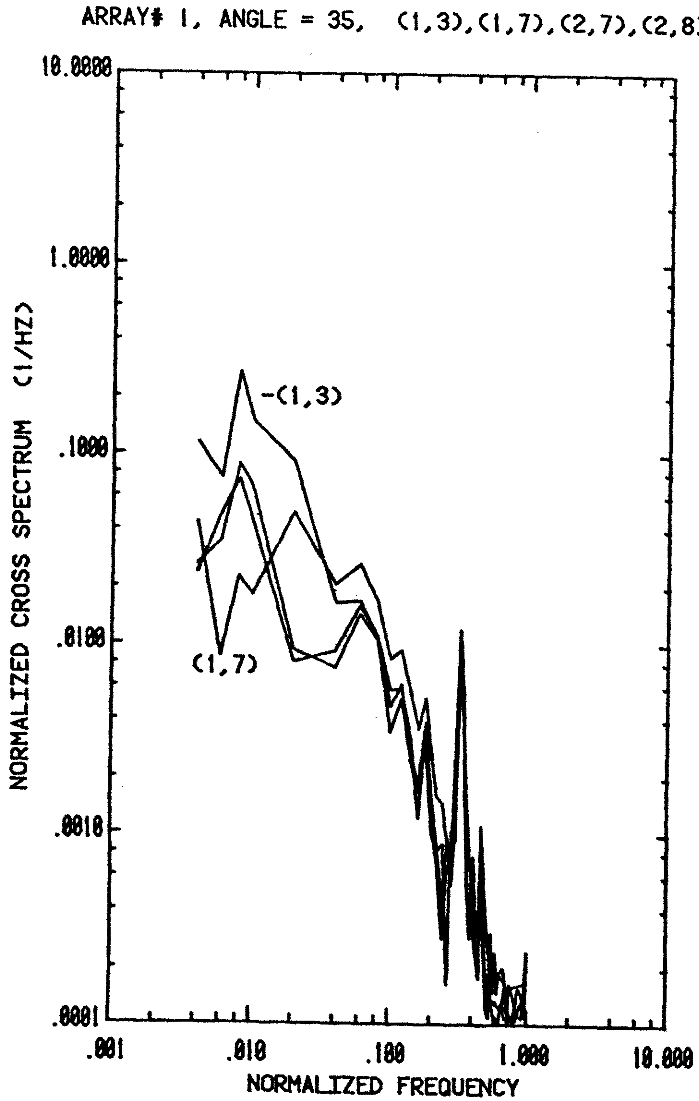

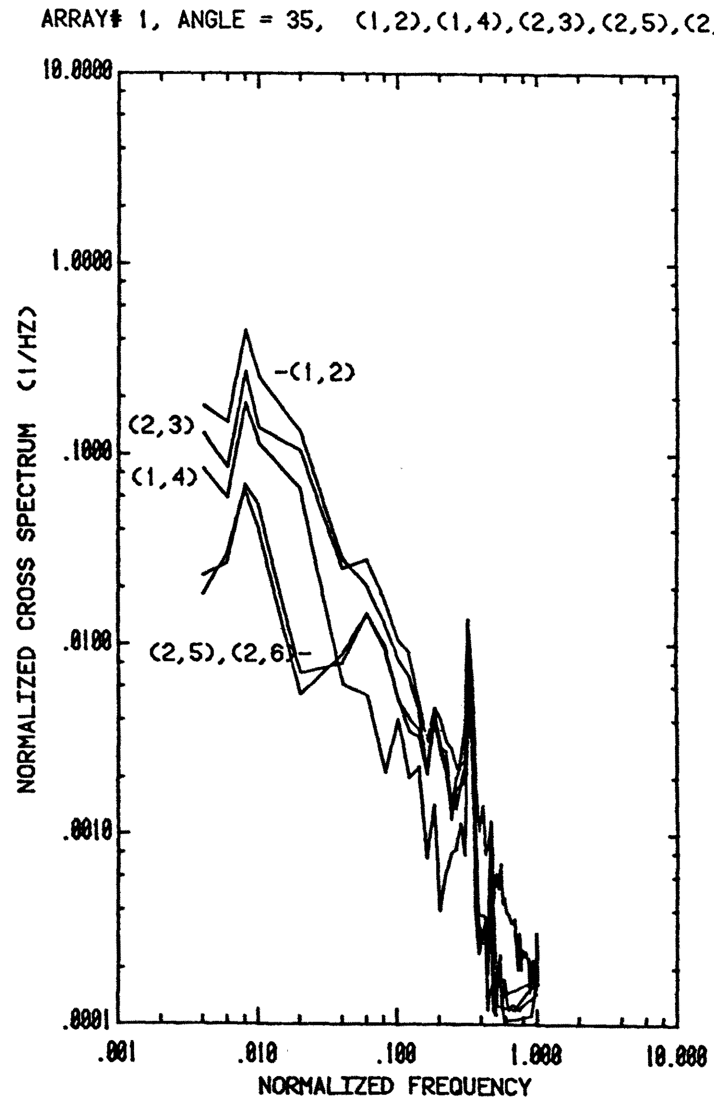

Figure 10. Cross-Spectra for First Array at $\alpha = 35°$, without Fence (continued)

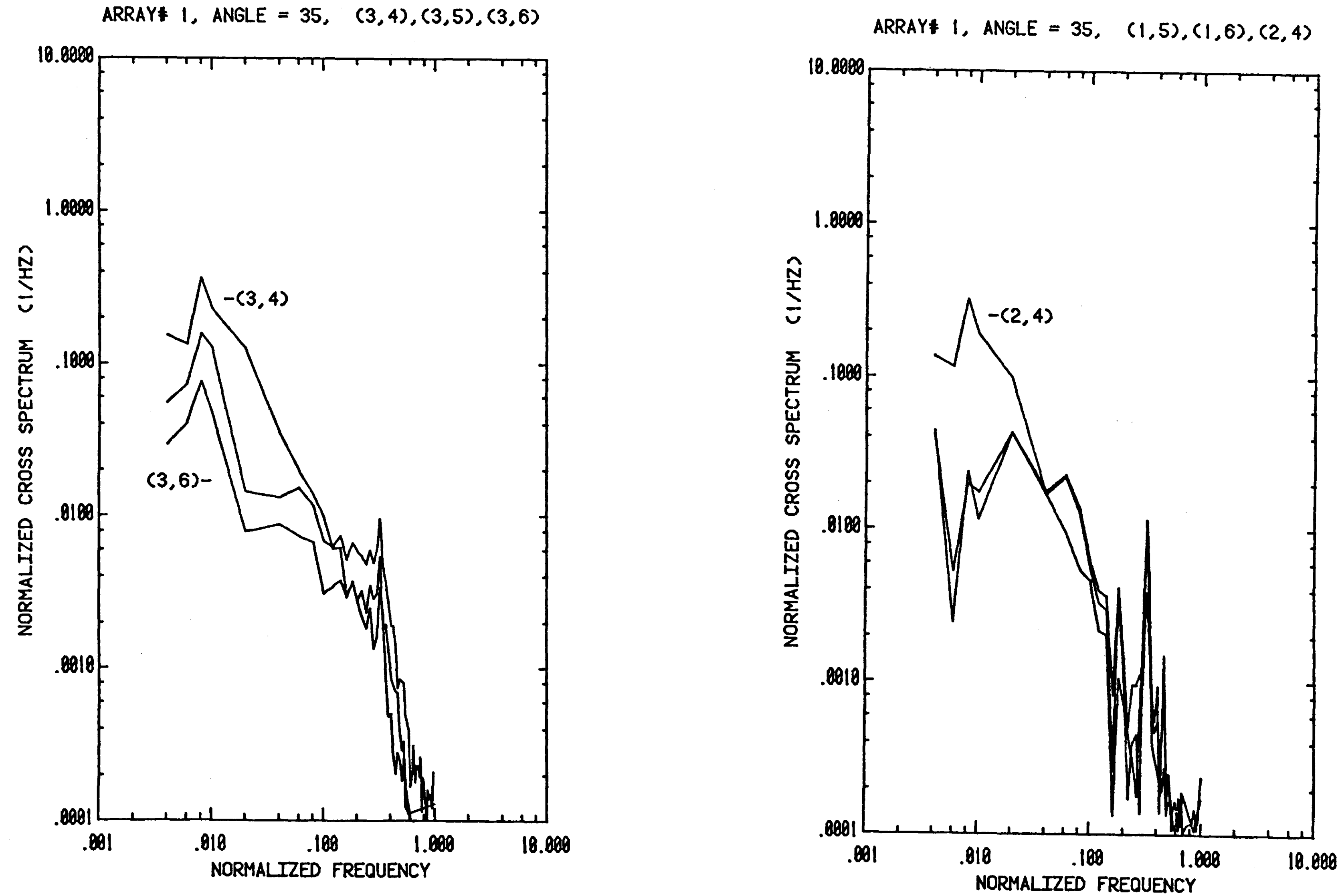

Figure 10. Cross-Spectra for First Array at $\alpha = 35°$, without Fence (continued)

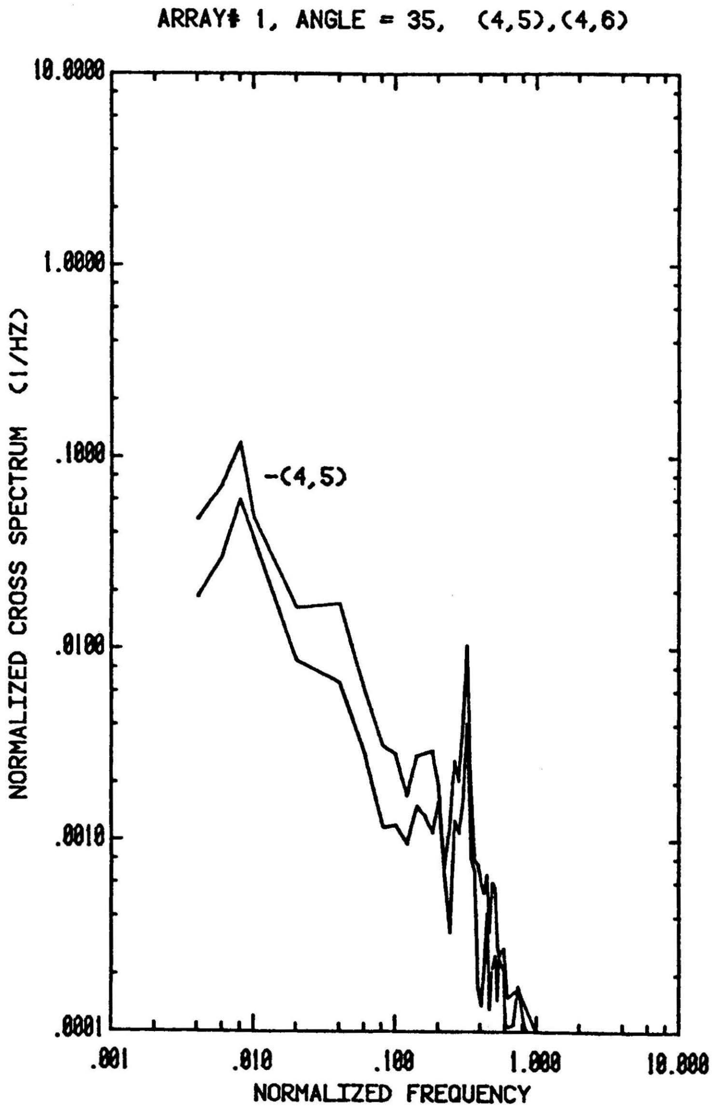

Figure 10. Cross-Spectra for First Array at α = 35°, without Fence (concluded)

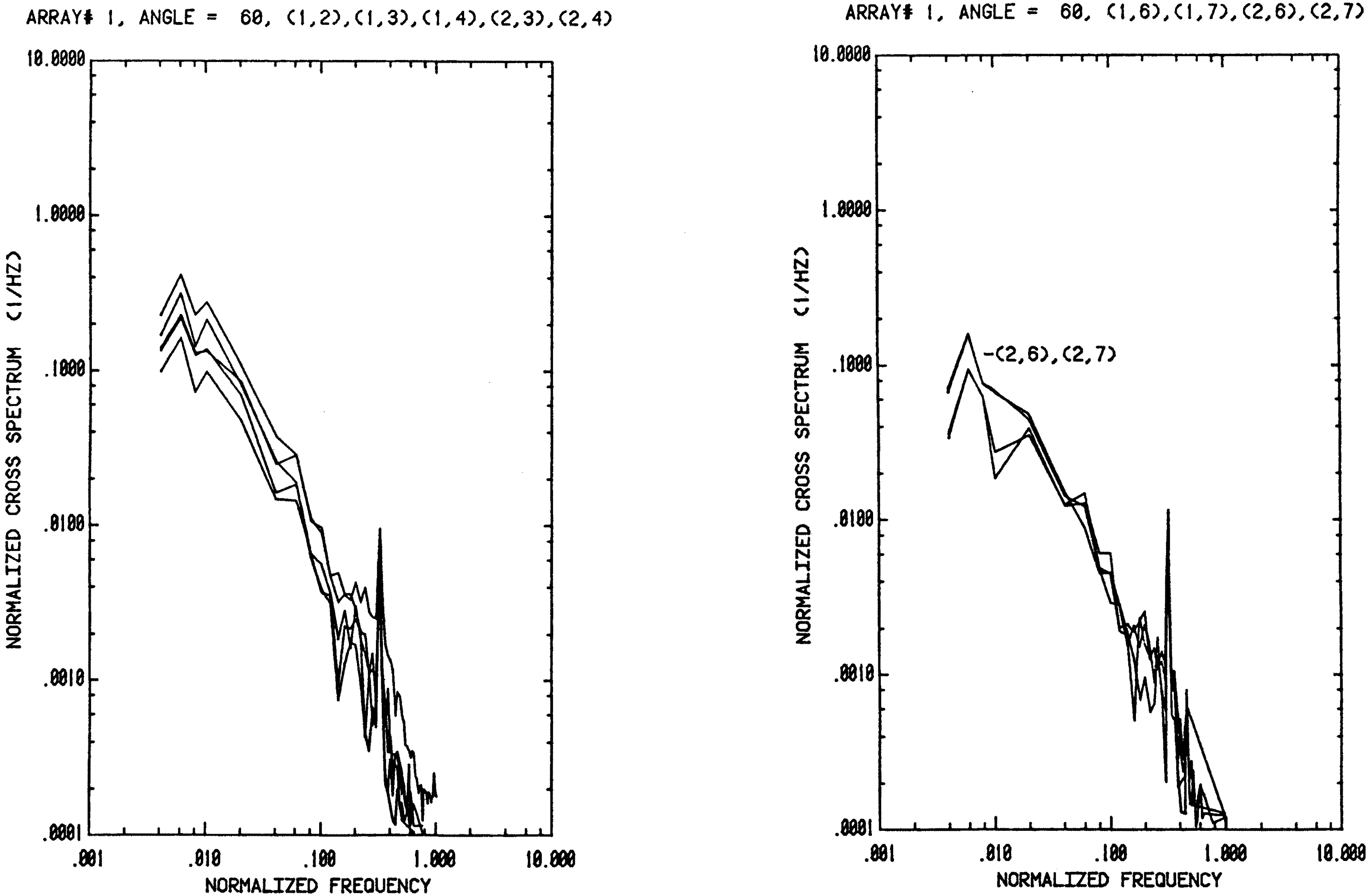

Figure 11. Cross-Spectra for First Array at α = 60°, without Fence

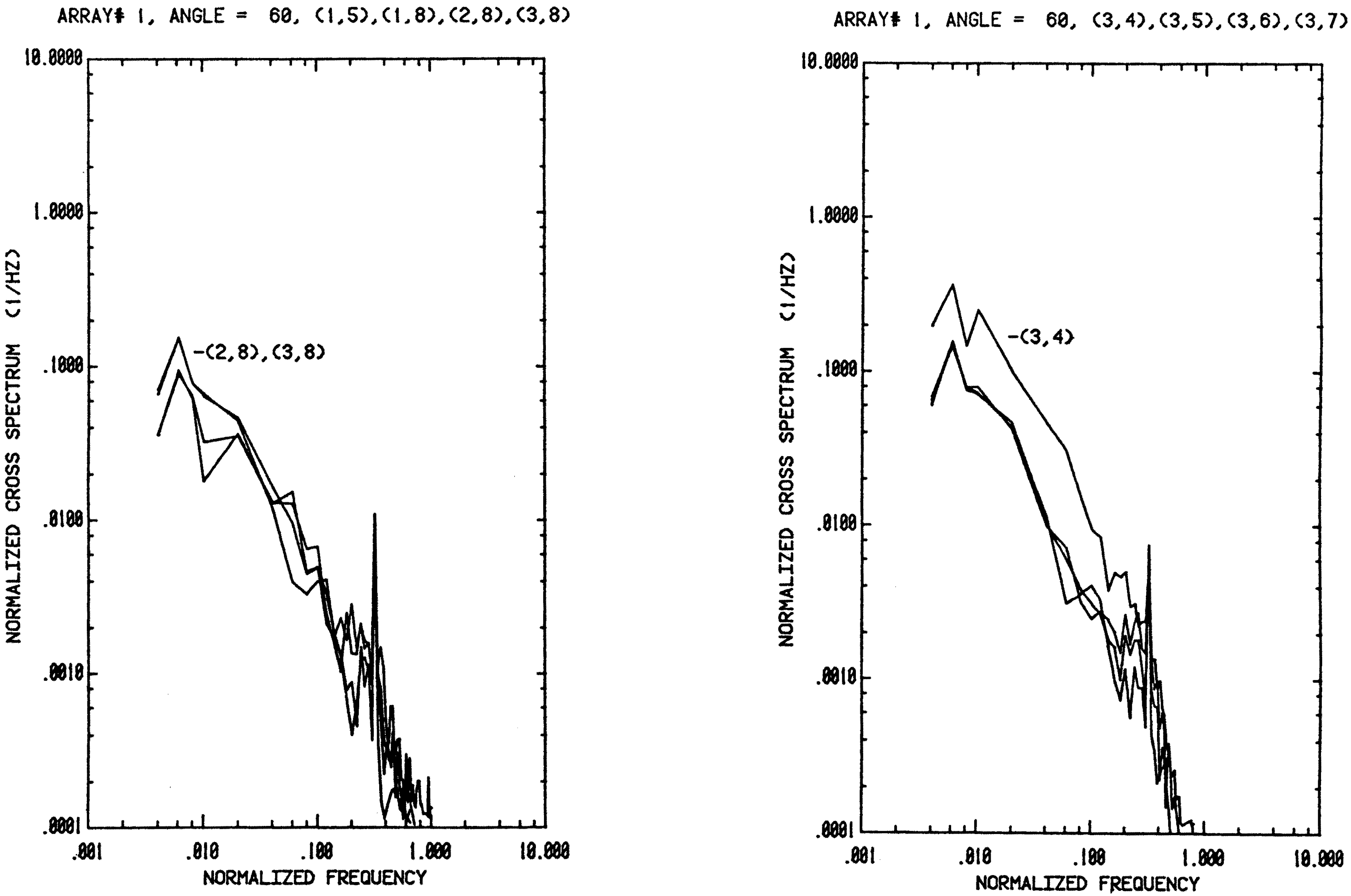

Figure 11. Cross-Spectra for First Array at $\alpha = 60°$, without Fence (continued)

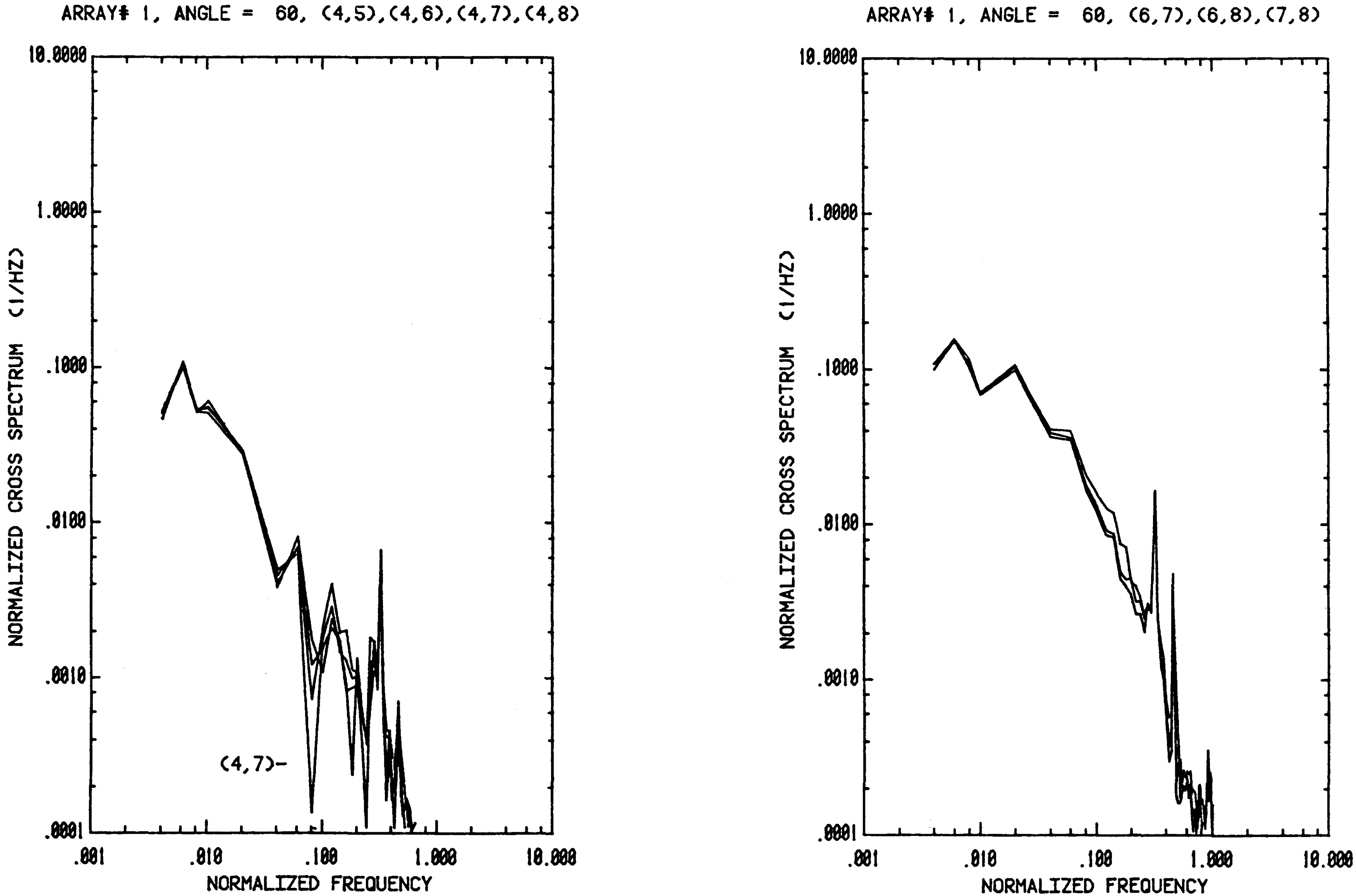

Figure 11. Cross-Spectra for First Array at $\alpha = 60°$, without Fence (continued)

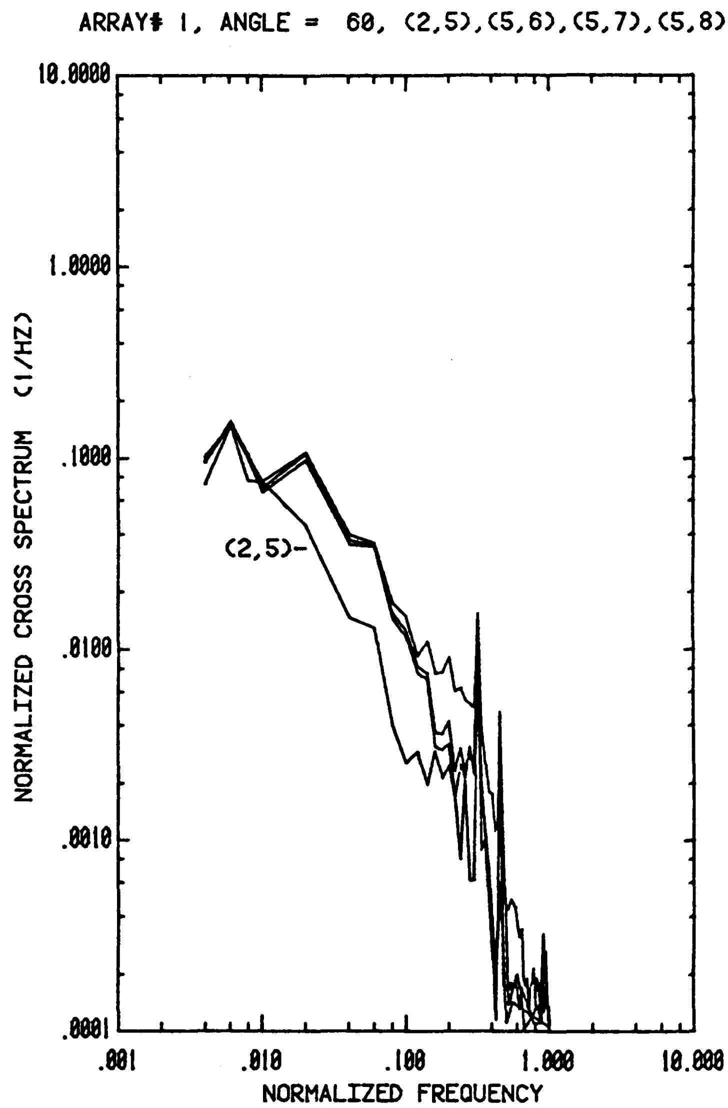

Figure 11. Cross-Spectra for First Array at $\alpha = 60°$, without Fence (concluded)

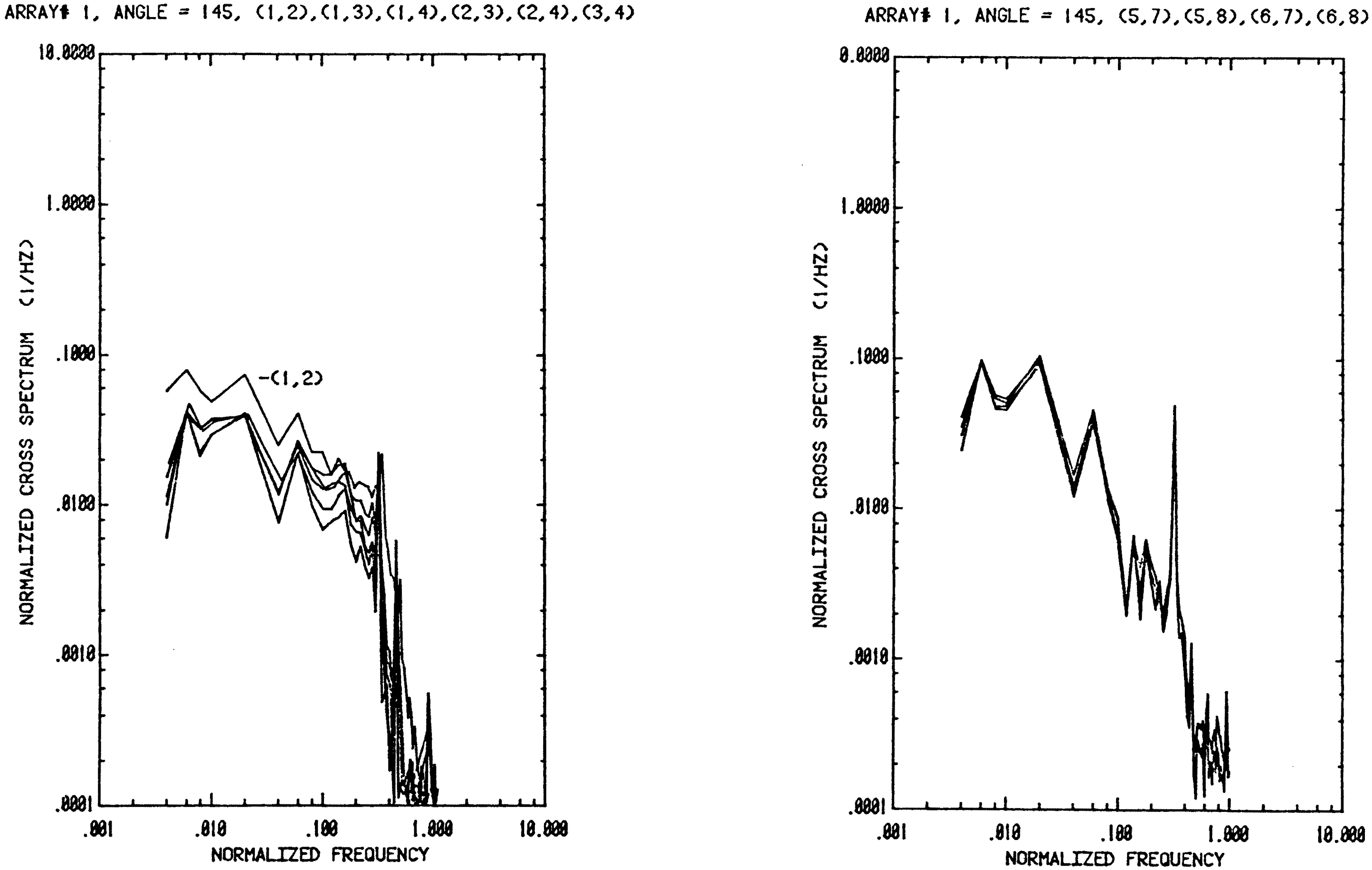

Figure 12. Cross-Spectra for First Array at α = 145°, with Fence

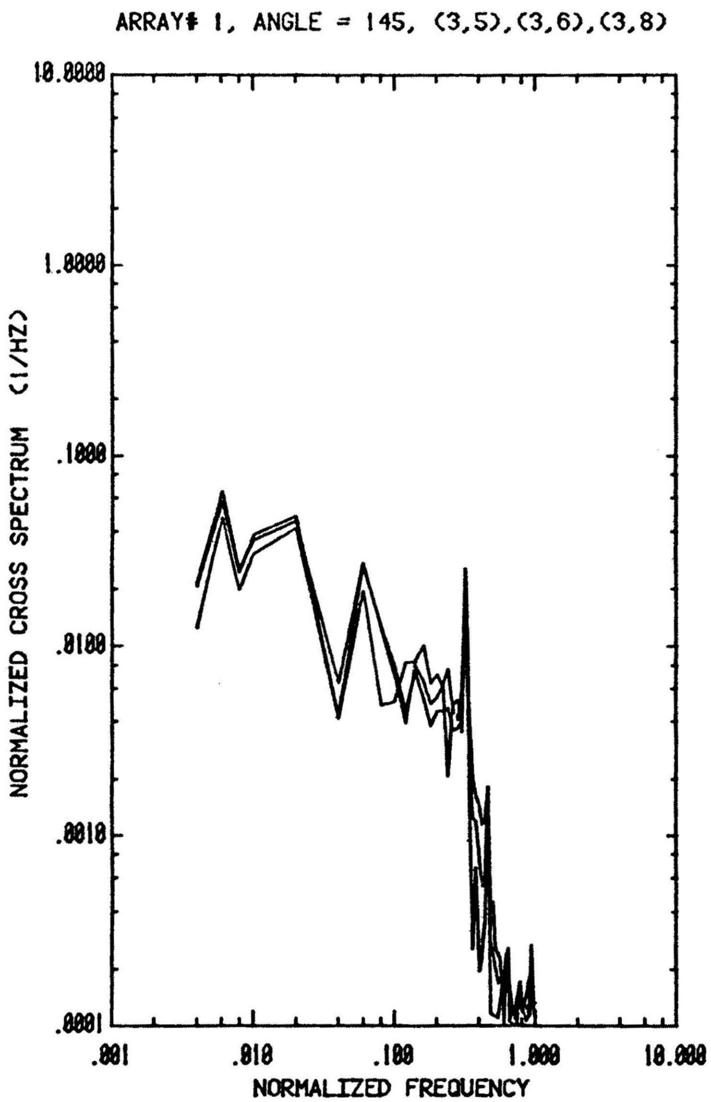

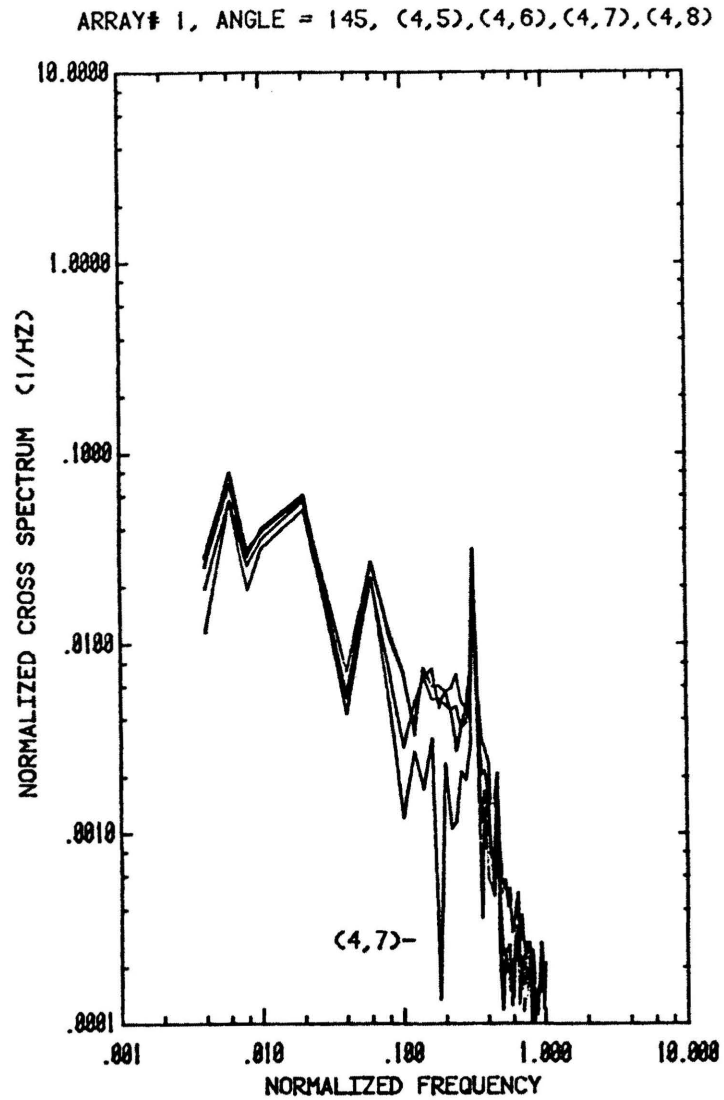

Figure 12. Cross-Spectra for First Array at $\alpha = 145°$, with Fence (continued)

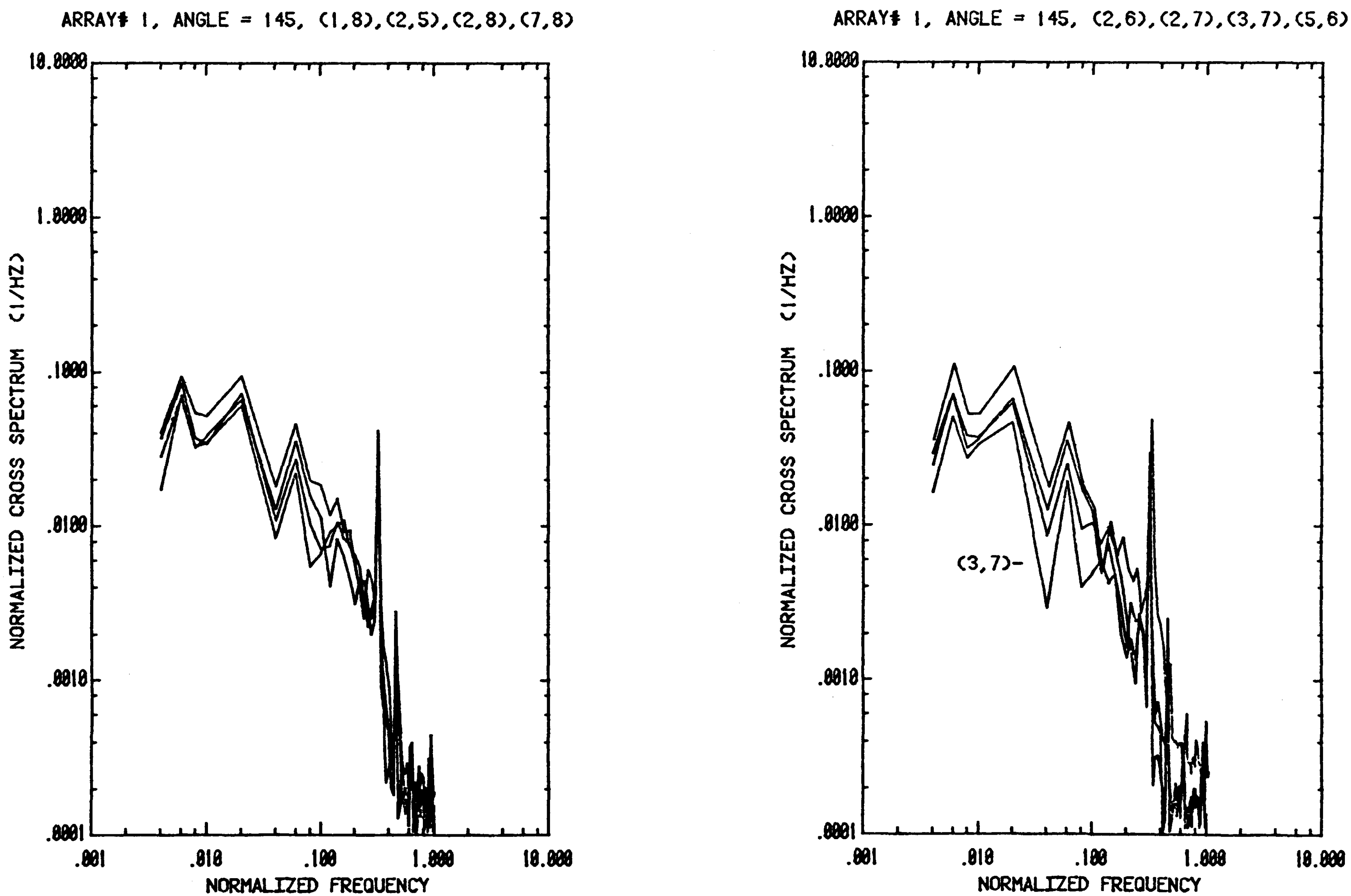

Figure 12. Cross-Spectra for First Array at α = 145°, with Fence (continued)

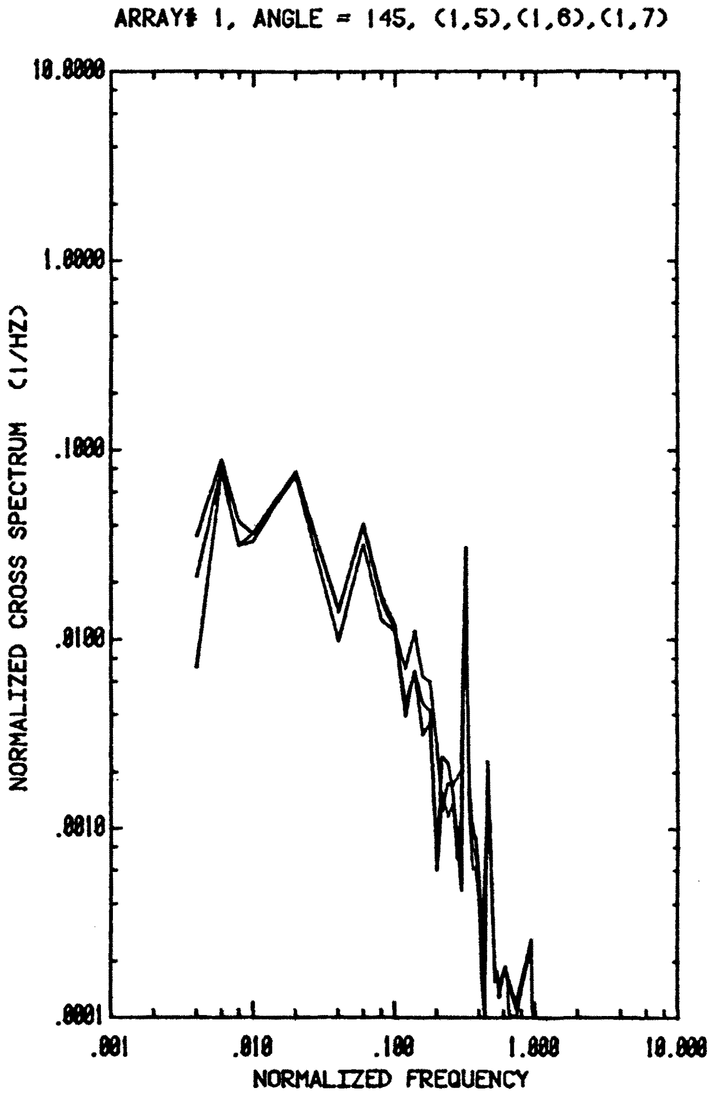

Figure 12. Cross-Spectra for First Array at α = 145°, with Fence (concluded)

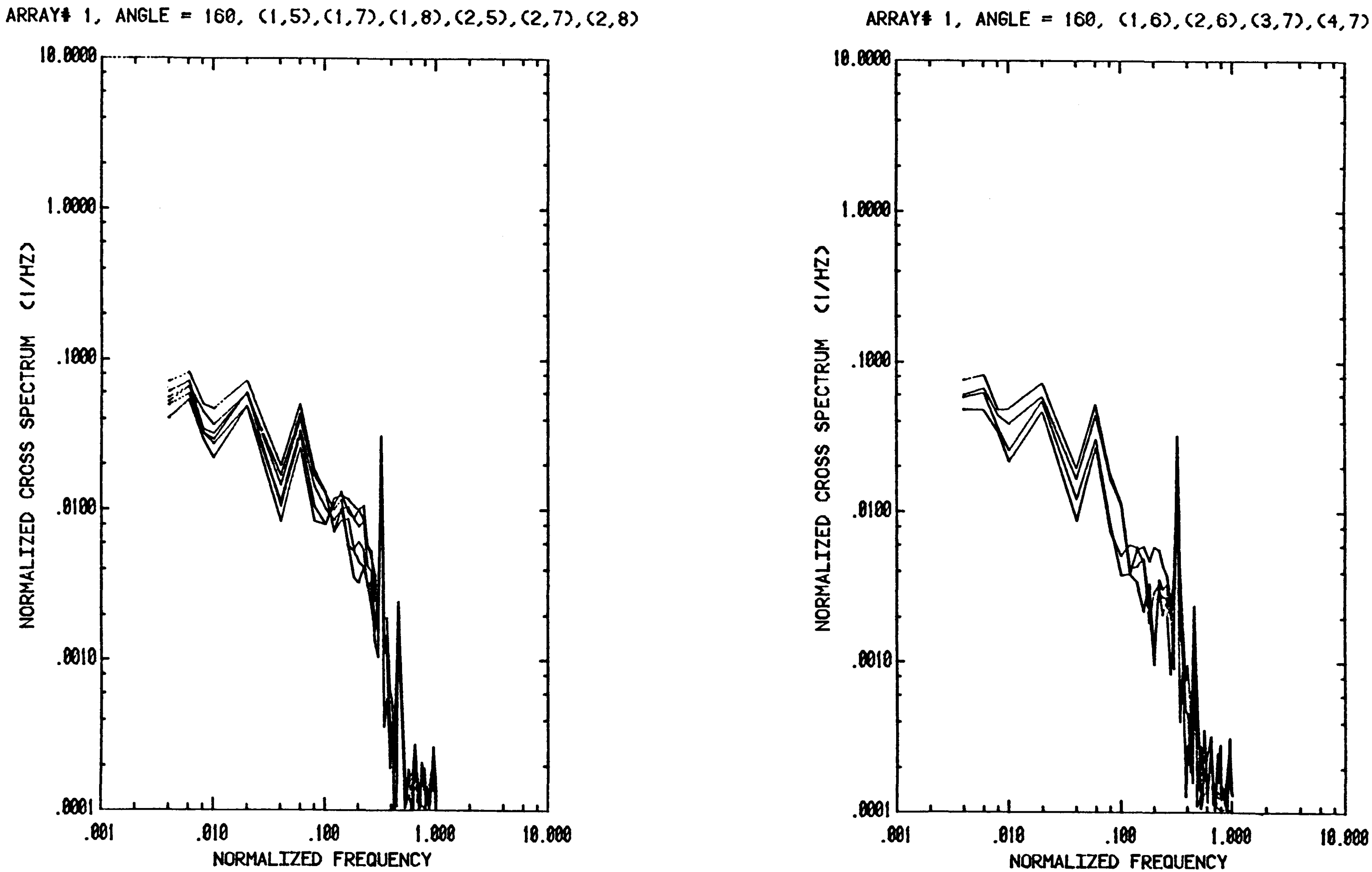

Figure 13. Cross-Spectra for First Array at α = 160°, with Fence

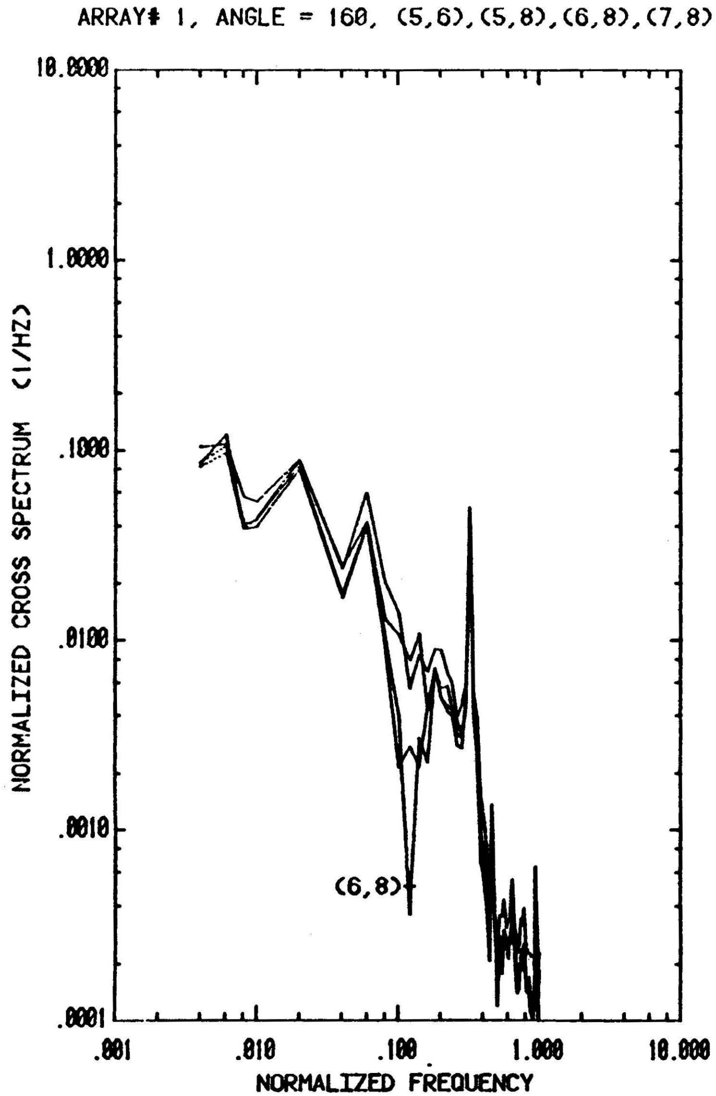

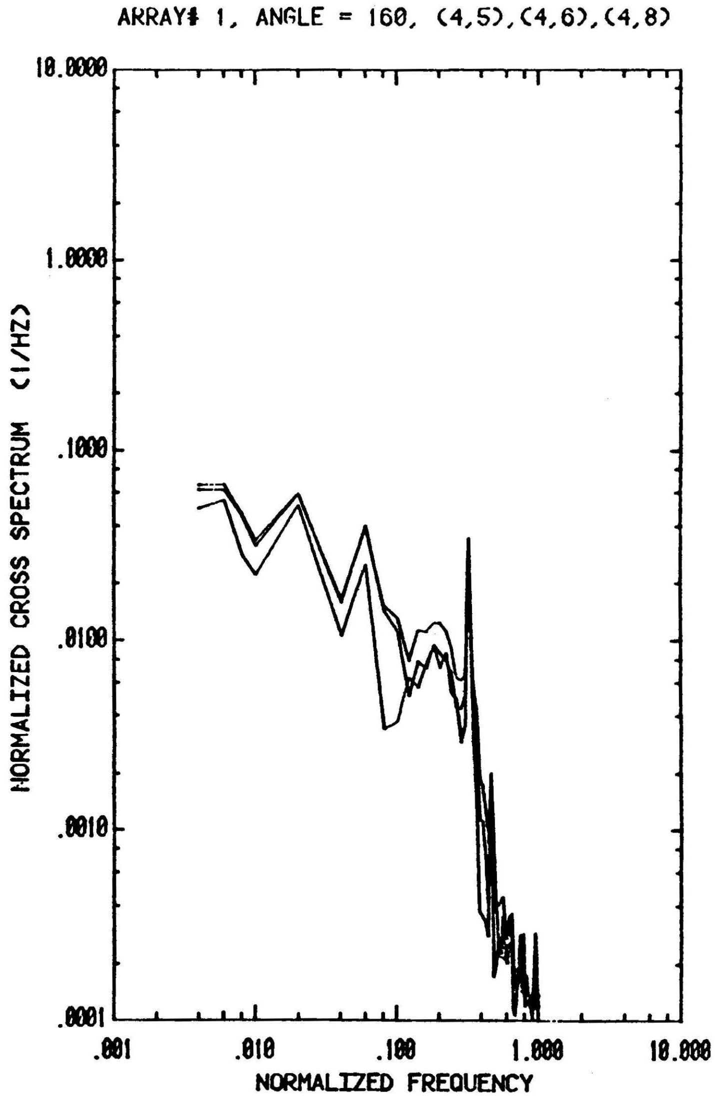

Figure 13. Cross-Spectra for First Array at α = 160°, with Fence (continued)

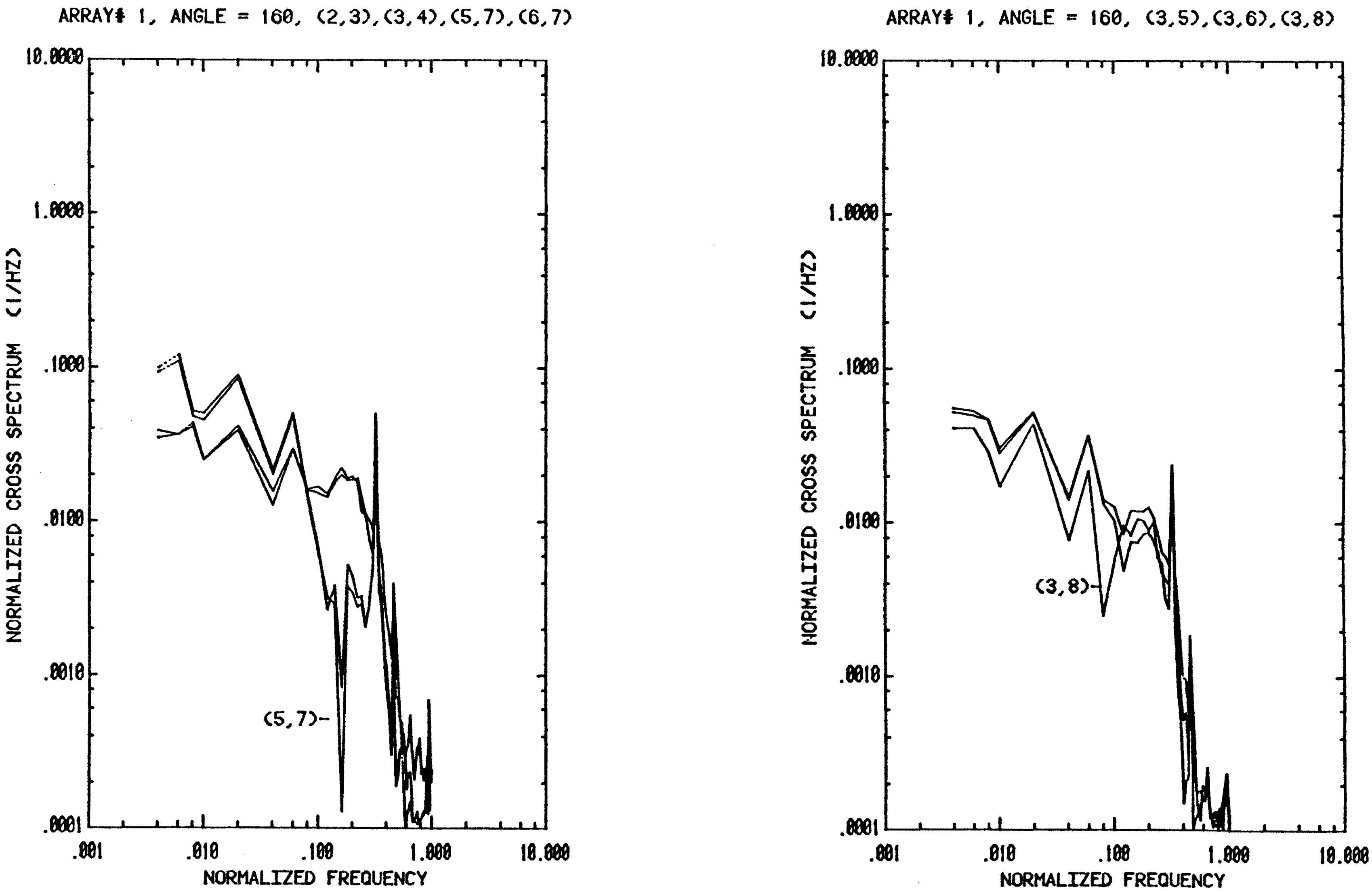

Figure 13. Cross-Spectra for First Array at α = 160°, with Fence (continued)

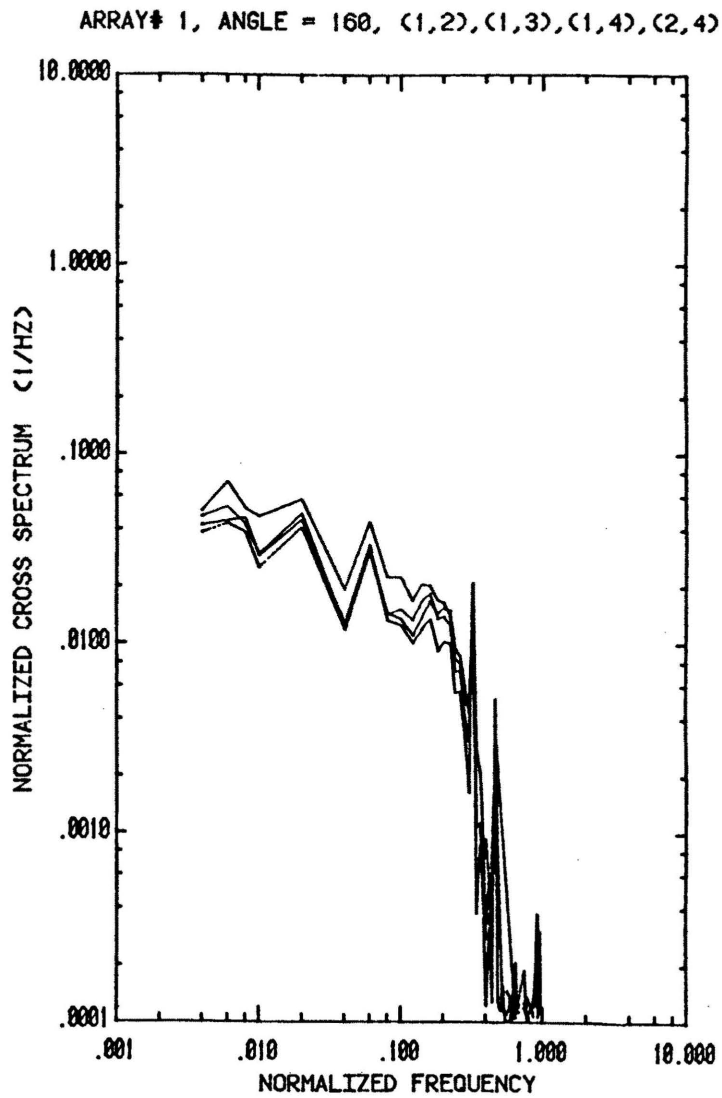

Figure 13. Cross-Spectra for First Array at α = 160°, with Fence (concluded)

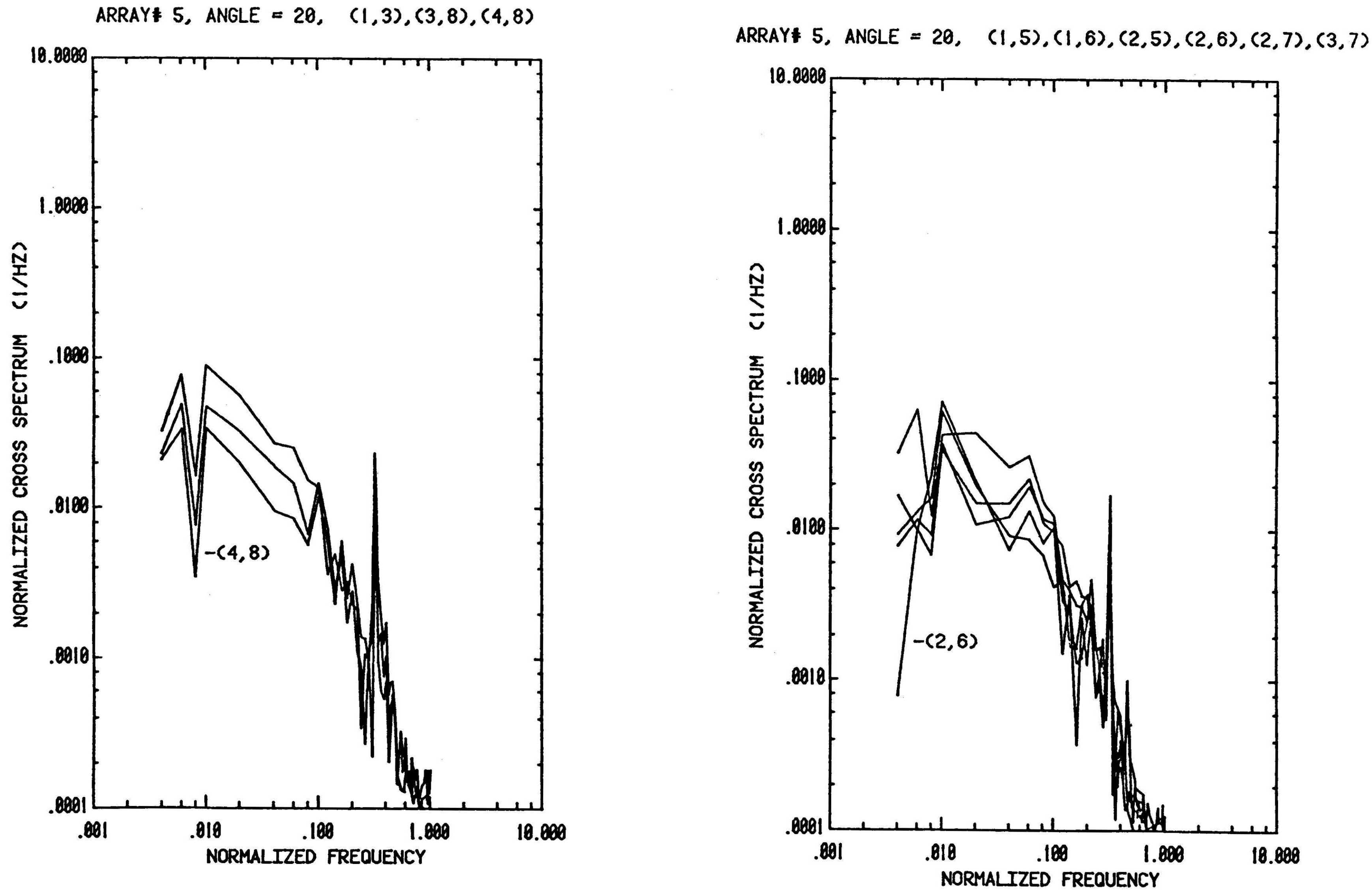

Figure 14. Cross-Spectra for Fifth Array at $\alpha = 20°$, without Fence

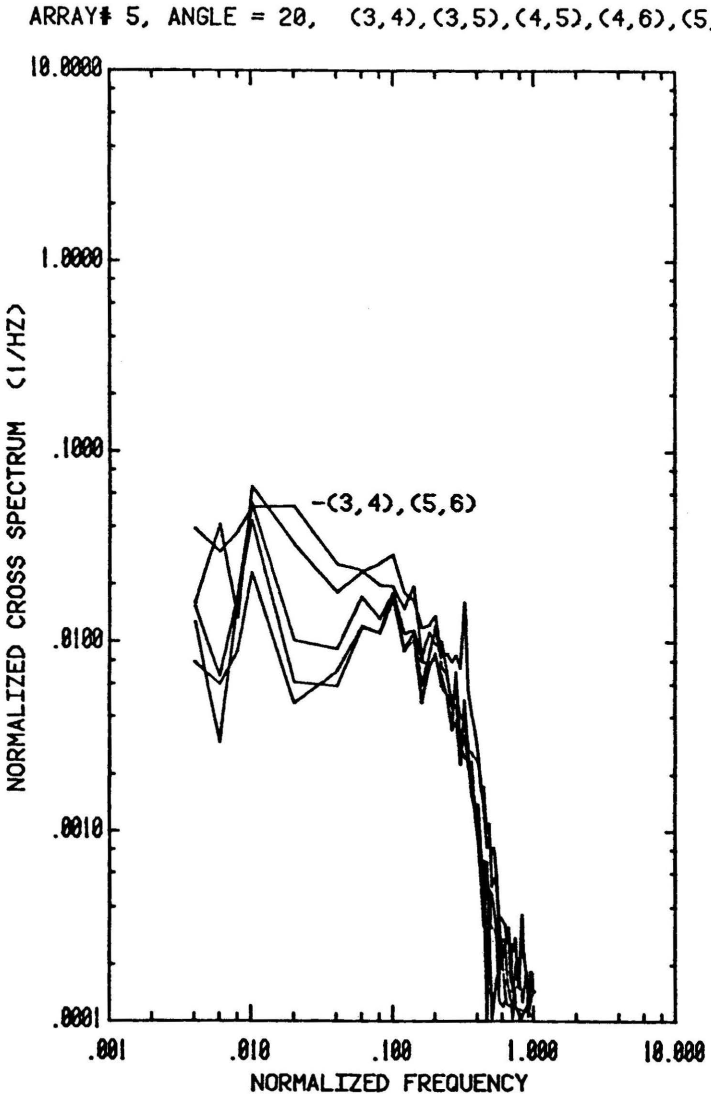

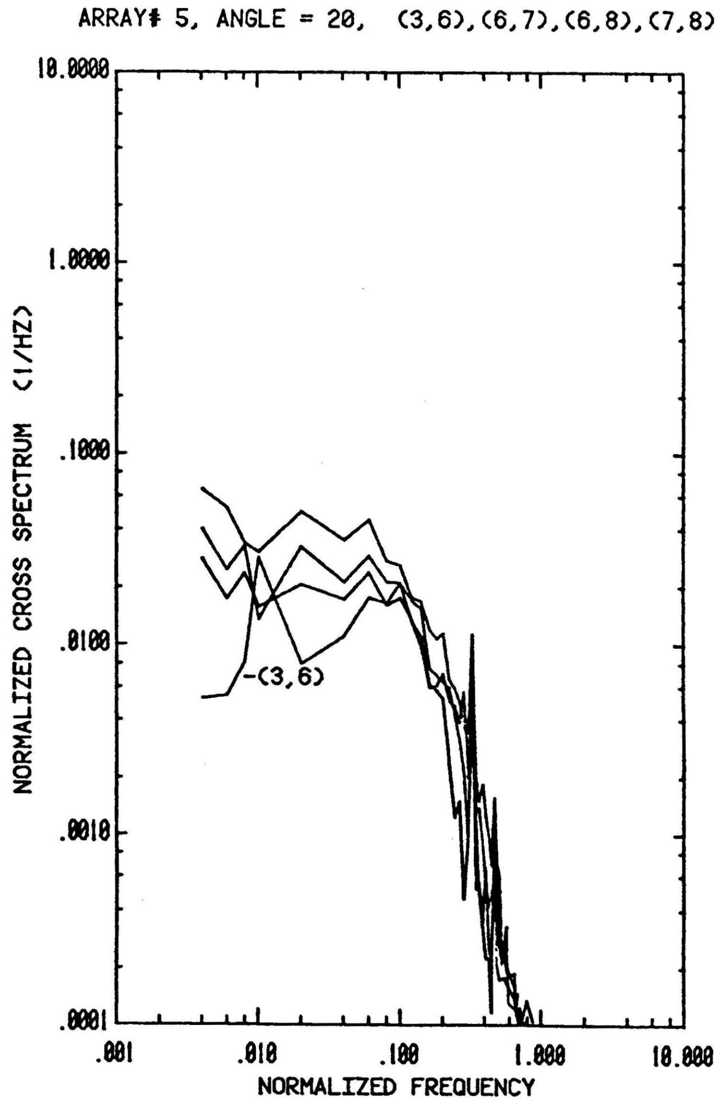

Figure 14. Cross-Spectra for Fifth Array at $\alpha = 20°$, without Fence
(continued)

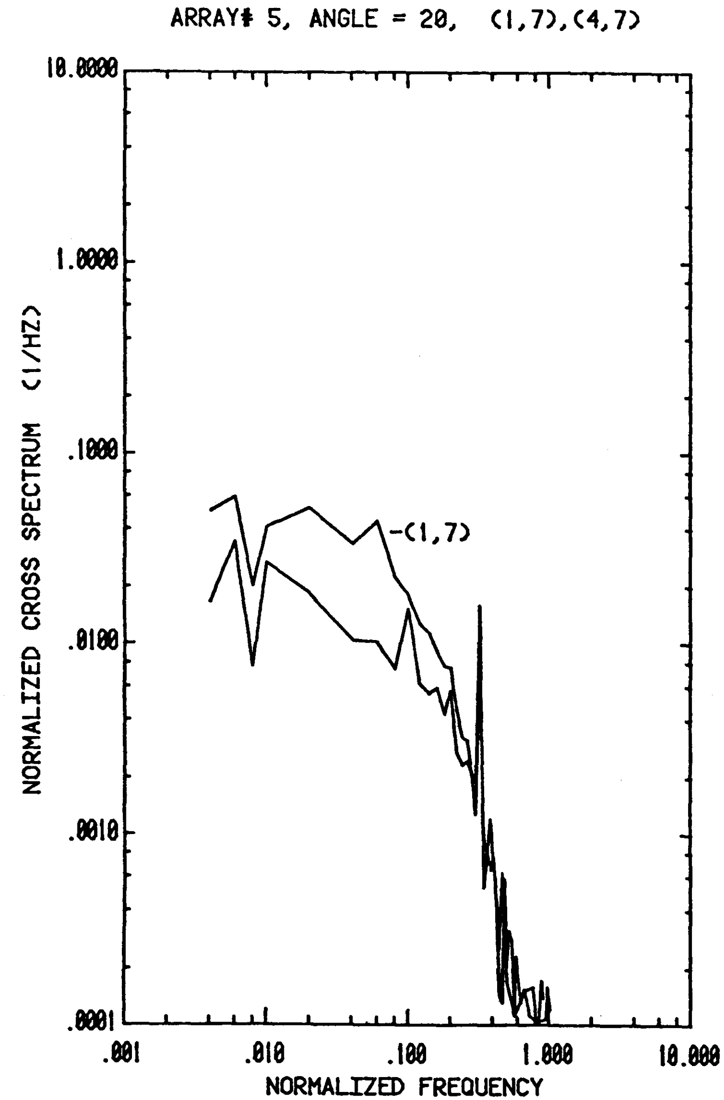

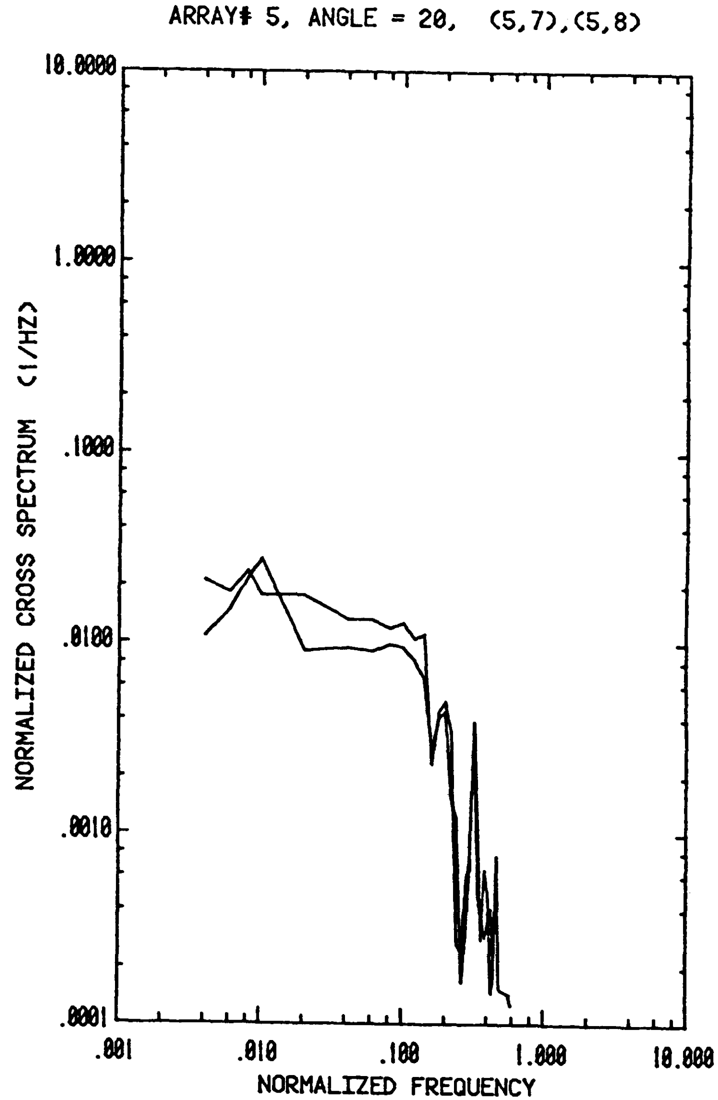

Figure 14. Cross-Spectra for Fifth Array at $\alpha = 20°$, without Fence (continued)

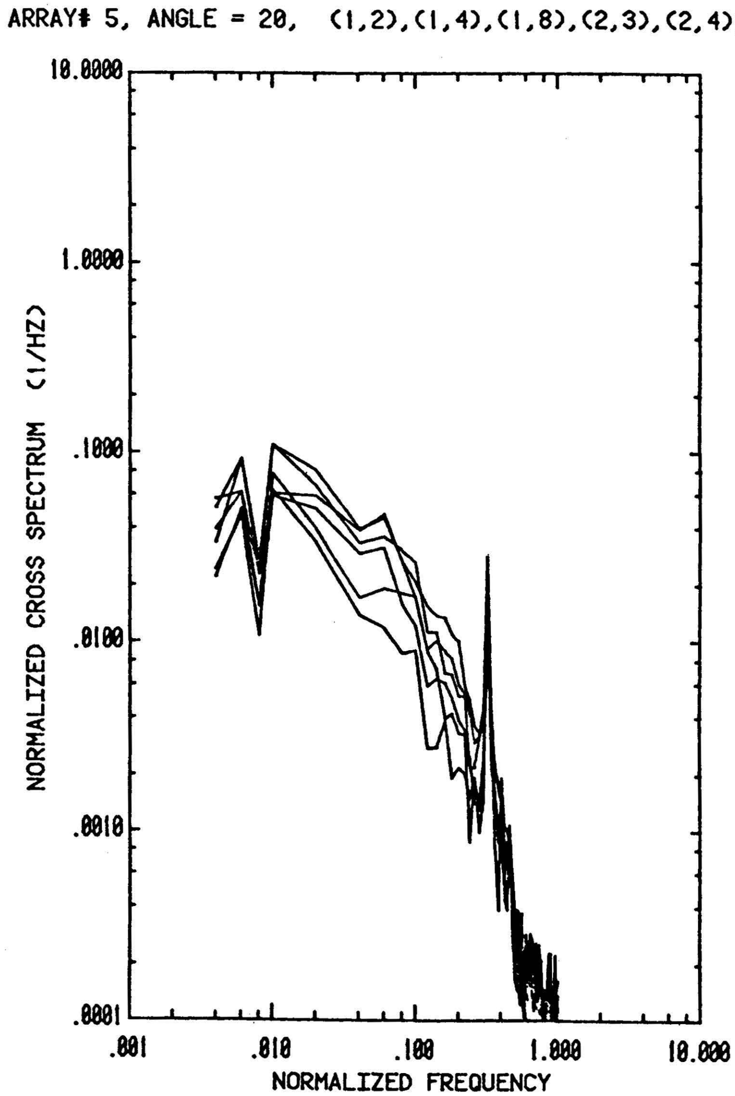

Figure 14. Cross-Spectra for Fifth Array at $\alpha = 20°$, without Fence (concluded)

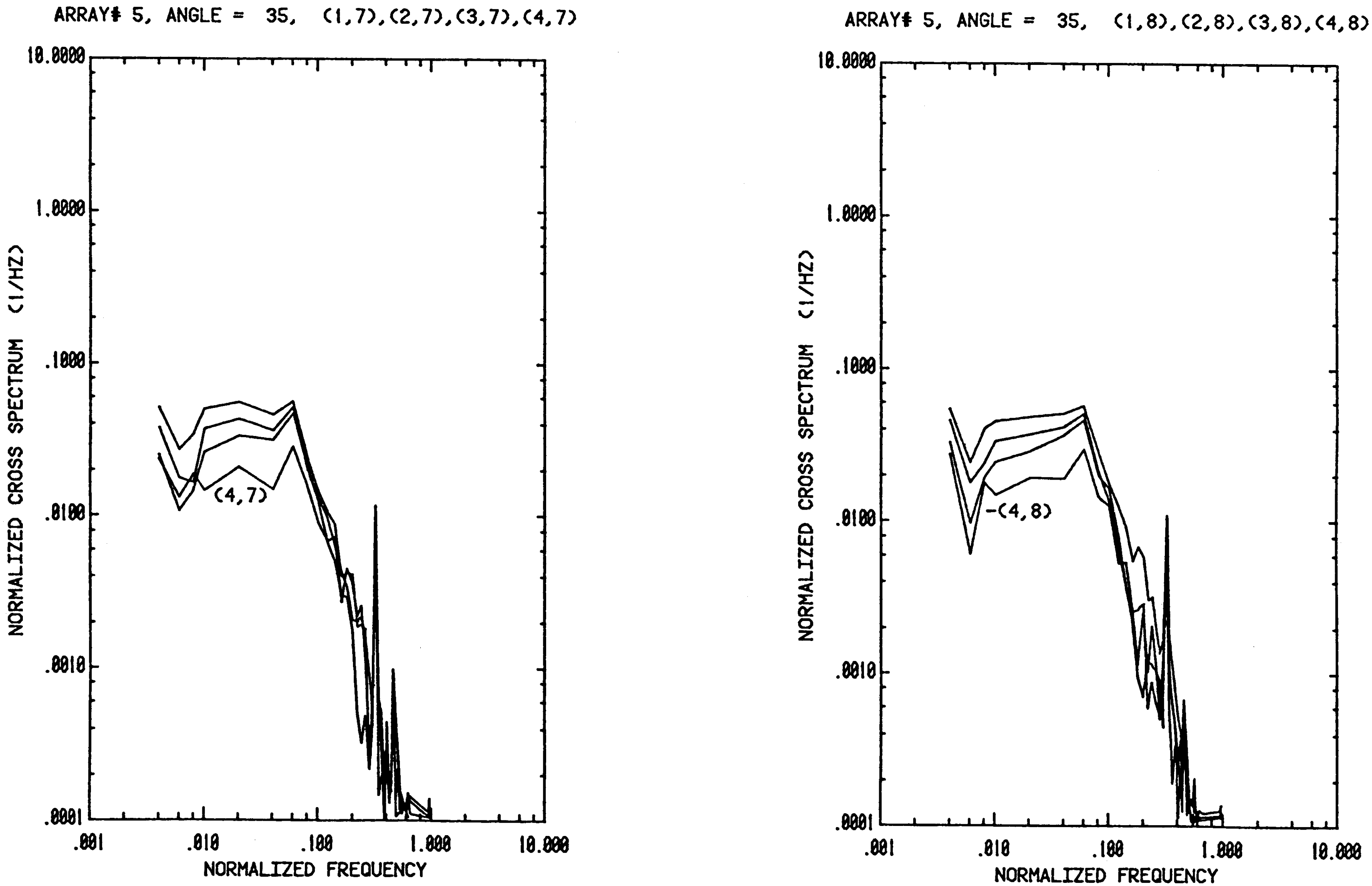

Figure 15. Cross-Spectra for Fifth Array at α = 35°, without Fence

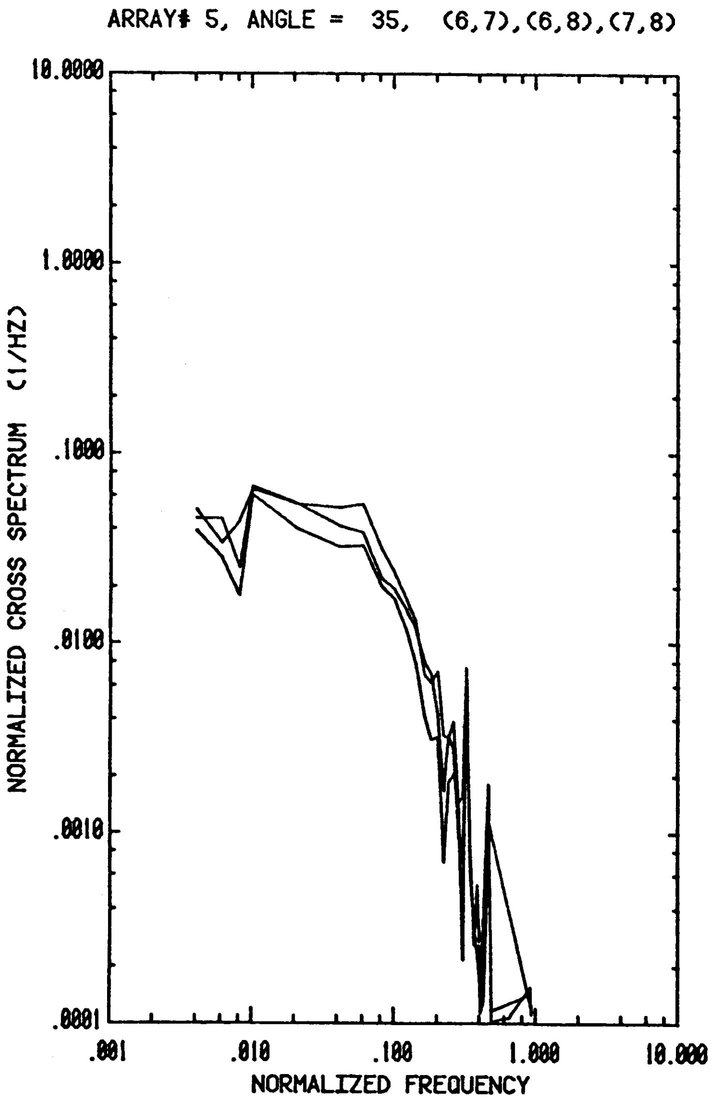

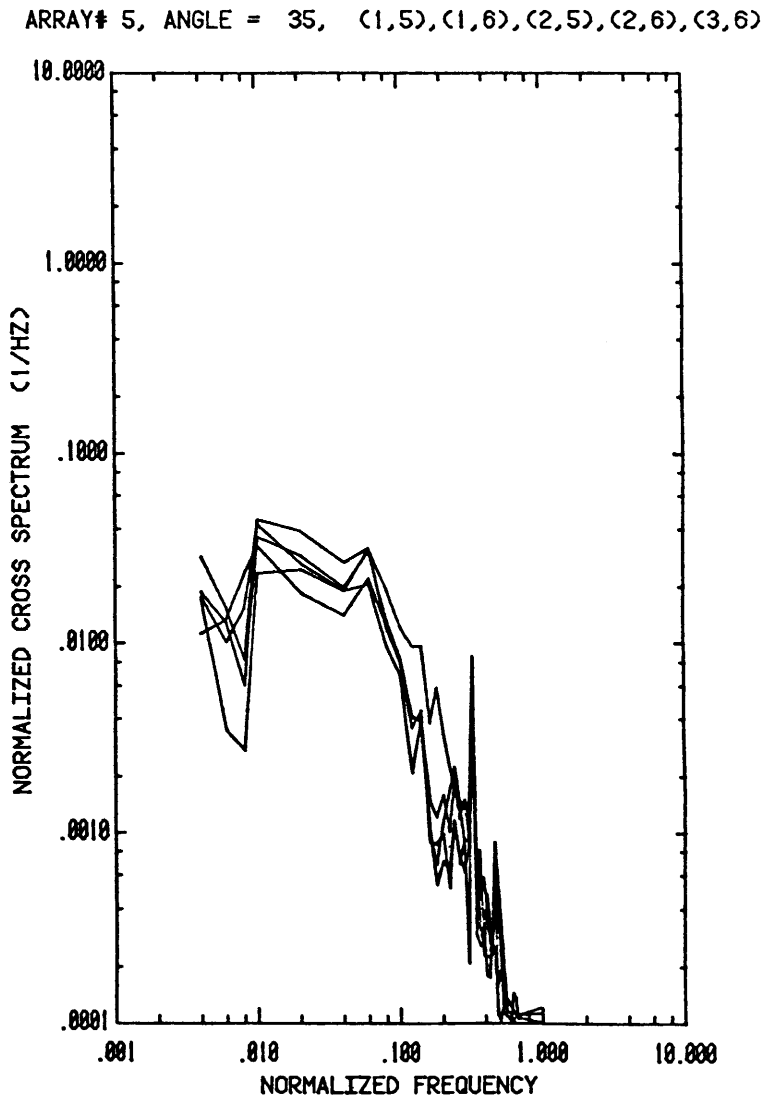

Figure 15. Cross-Spectra for Fifth Array at $\alpha = 35°$, without Fence (continued)

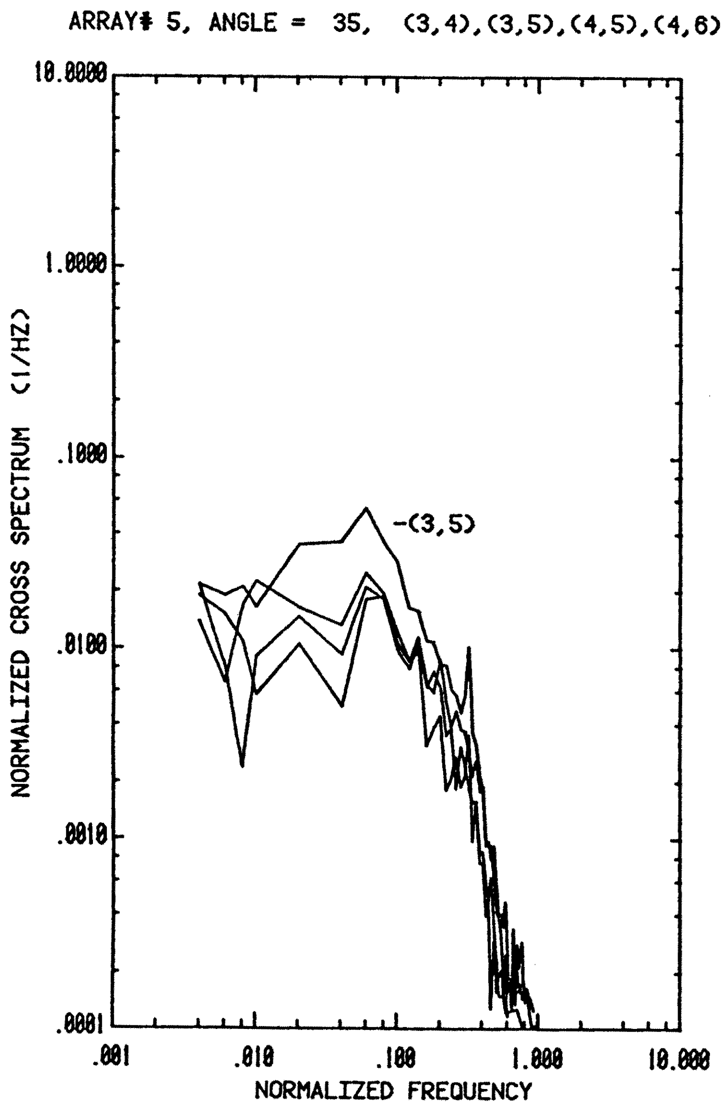

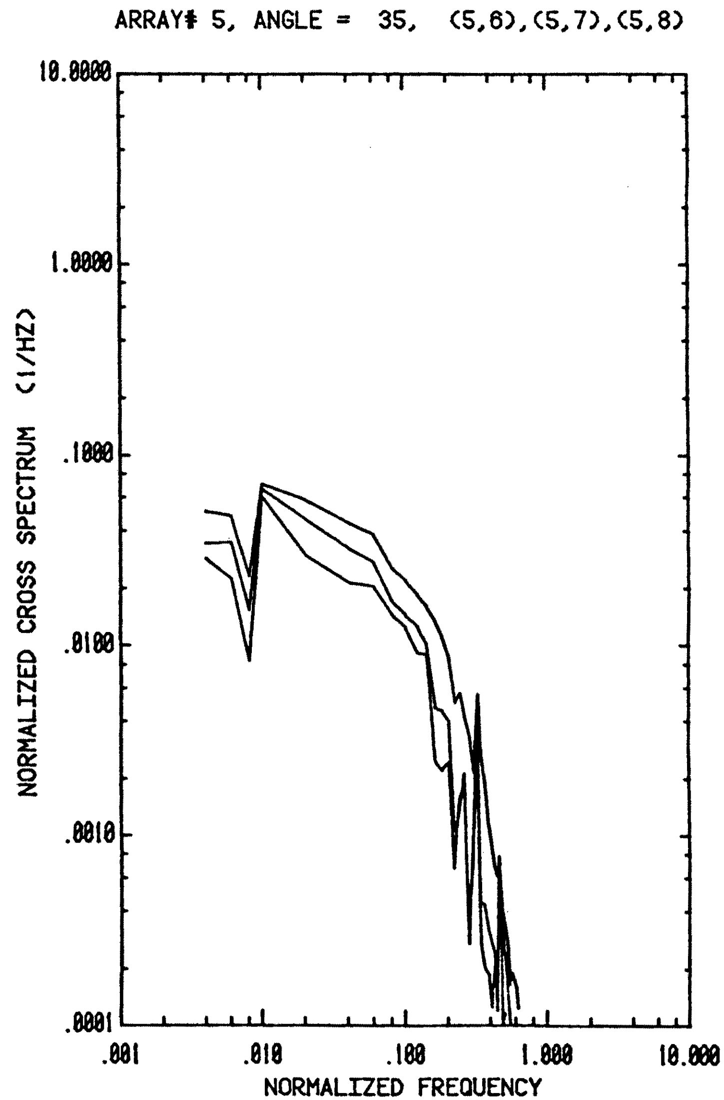

Figure 15. Cross-Spectra for Fifth Array at $\alpha = 35°$, without Fence (continued)

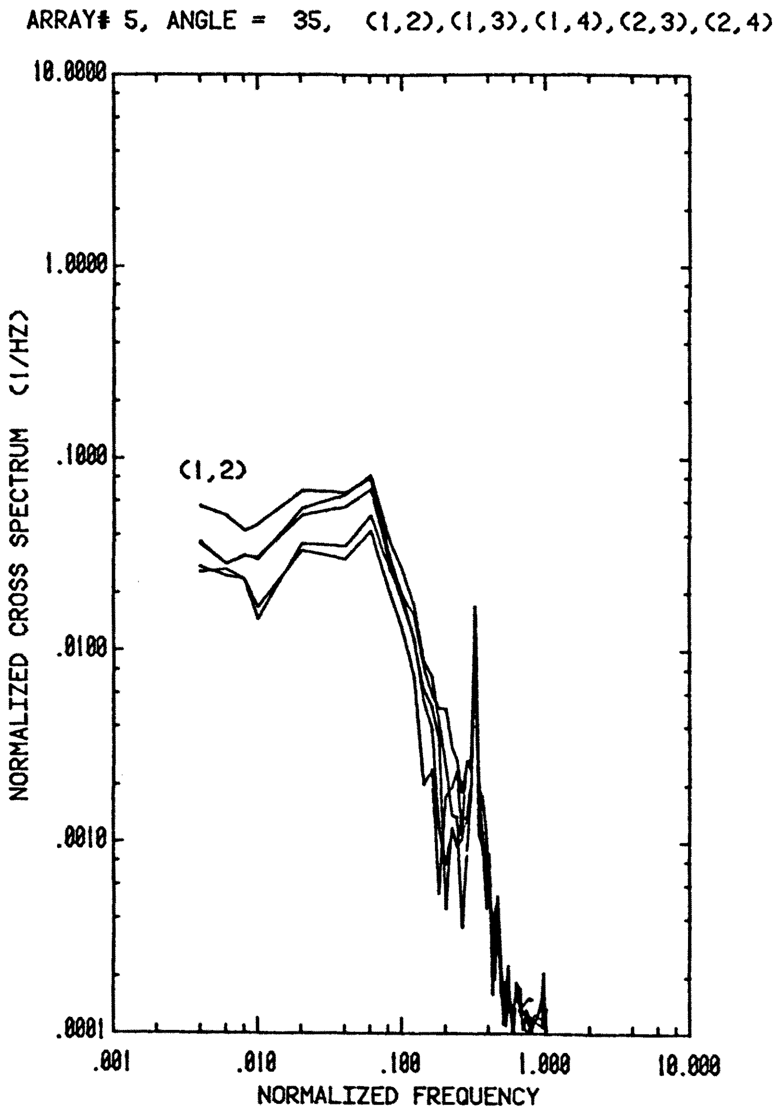

Figure 15. Cross-Spectra for Fifth Array at $\alpha = 35°$, without Fence (concluded)

TABLES

Table 1. List of Array Configurations Tested

Run	α	Array	Fence**		
			Height (H_f/c)	Distance (x_f/c)	Porosity (%)
21318	120	5	--	--	--
21321	120	1	--	--	--
21323	120	1	0.75	2.5	30
21325	145	5	--	--	--
21327	145	2	--	--	--
21329	145	1	--	--	--
21331	145	1	0.75	2.5	30
21338*	145	1	--	--	--
21340	160	5	--	--	--
21342	160	1	--	--	--
21344	160	1	0.75	2.5	30
21346	20	5	--	--	--
21348	20	1	--	--	--
21350	20	1	0.75	2.5	30
21352	35	5	--	--	--
21354	35	2	--	--	--
21356	35	1	--	--	--
21358	35	1	0.75	2.5	30
21364*	35	1	--	--	--
21366	60	5	--	--	--
21368	60	1	--	--	--
21370	60	1	0.75	2.5	30

*edge study (see Section 2.3 of the preceding report for the definition)
**see Figure 2 for definition of parameters

Table 2a. Time-Averaged Pressure Coefficients

	Run 21331*		Run 21344*		Run 21346	
	α	Array	α	Array	α	Array
	145	1	160	1	20	5
Tap (original)	$C_{P_{mean}}$	$C_{P_{rms}}$	$C_{P_{mean}}$	$C_{P_{rms}}$	$C_{P_{mean}}$	$C_{P_{rms}}$
1 (1)	-.083	.051	-.105	.052	.020	.051
2 (4)	-.068	.057	-.096	.061	.055	.050
3 (7)	-.088	.078	-.133	.072	.075	.069
4 (10)	-.107	.068	-.109	.060	.077	.113
5 (11)	-.134	.040	-.096	.040	-.196	.210
6 (14)	-.136	.039	-.096	.038	-.116	.121
7 (17)	-.153	.042	-.121	.042	-.103	.078
8 (20)	-.131	.044	-.107	.045	-.054	.072

*with fence

Table 2b. Time-Averaged Pressure Coefficients

	Run 21352		Run 21356		Run 21368	
	α	Array	α	Array	α	Array
	35	5	35	1	60	1
Tap (original)	$C_{P_{mean}}$	$C_{P_{rms}}$	$C_{P_{mean}}$	$C_{P_{rms}}$	$C_{P_{mean}}$	$C_{P_{rms}}$
1 (1)	-.013	.060	.087	.054	.223	.089
2 (4)	.001	.062	.292	.067	.376	.095
3 (7)	-.004	.081	.436	.107	.482	.148
4 (10)	-.002	.120	.451	.178	.279	.177
5 (11)	-.140	.147	-.300	.081	-.417	.066
6 (14)	-.104	.109	-.290	.073	-.398	.063
7 (17)	-.126	.089	-.346	.071	-.472	.063
8 (20)	-.092	.097	-.293	.072	-.417	.064

Table 3. Comparison of Integration of Auto-Spectra

array = 1, α = 35°, without fence	
pressure taps	$\int^{*} \Phi_{ii}(N)dN/C^2_{p_{rms_i}}$
(1, 1)	0.990
(2, 2)	1.069
(3, 3)	1.165
(4, 4)	1.059
(5, 5)	1.004
(6, 6)	0.971
(7, 7)	0.986
(8, 8)	0.963

array = 5, α = 35°, without fence	
(1, 1)	1.035
(2, 2)	1.016
(3, 3)	1.070
(4, 4)	0.986
(5, 5)	1.061
(6, 6)	1.061
(7, 7)	0.991
(8, 8)	0.972

*by theory, this quantity should be identically equal to 1 (see Equation 8)